

Theory of strain induced anisotropic resistivity of extremely strongly correlated metals in two dimensions

Michael Arciniaga¹, Peizhi Mai^{2,1}, B Sriram Shastry¹

¹Physics Department, University of California, Santa Cruz, CA 95064, USA and

²Center for Nanophase Materials Sciences, Oak Ridge National Laboratory, Oak Ridge, TN, 37831-6494, USA

(Dated: May 19, 2022)

We present theoretical results for the effect of strain on resistivity, optical weight and local density of states using the recently developed extremely strongly correlated Fermi liquid theory in two dimensions. The strain induced variations are obtained for a two-dimensional t - t' - J model, where t and t' are the first and second neighbor hopping parameters. Our calculation provides quantitative predictions for these quantities. These have the prospect of experimental tests in the near future, for strongly correlated materials such as the hole-doped and electron-doped high- T_c materials.

I. INTRODUCTION & MOTIVATION

Understanding the temperature and doping dependent electrical conductivity of very strongly correlated metals in two dimensions is a very important problem in condensed matter physics. This problem has been explored in various experiments¹⁻³ on different materials over last few decades. Experiments reveal interesting and challenging transport regimes, termed the *strange metal* and the *bad metal* regime, whose existence is inexplicable within the standard Fermi liquid theory of metals. These results have attracted several numerical studies using the techniques of dynamical mean field theory⁴⁻⁶, determinant quantum Monte-Carlo method^{7,8} and dynamical cluster approximation^{9,10} etc. These studies indicate that the unusual regimes are indicative of very strong correlations of the Mott-Hubbard variety.

Despite the numerical progress, few analytical techniques are available to extract the low temperature transport behavior, and thus better understand the various regimes. This is due to the inherent difficulties of treating strong correlations, i.e. physics beyond the scope of perturbation theory. Recently, the extremely correlated Fermi liquid theory (ECFL)^{11,28,29} has been developed by Shastry and coworkers. This theory consists of a basic reformulation of strong correlation physics, and its many applications have been reported for the t - t' - J model in dimensions $d=1,2,\infty$. This is a minimal and fundamental model to describe extreme correlations. The ECFL theory leads to encouraging results which are in close accord with experiments such as spectral line shape in angle-resolved photoemission spectroscopy (ARPES)^{12-17,31}, Raman susceptibility^{18,19}, and particularly, resistivity^{11,20,31,32}. ECFL theory gives a good account of the T and density dependence of the resistivity^{11,20,31,32} for hole-doped and electron-doped correlated materials.

In the ECFL theory, the resistivity arises from (umklapp-type) inelastic scattering between strongly correlated electrons. Here the hopping amplitudes of electrons play a dual role. The first one, that of propagating the fragile quasiparticles, is standard in all electronic systems- they model the band structure. Additionally,

for very strong correlations the ECFL theory shows that the hopping parameters are also involved in the scattering of quasiparticles off each other. This can be seen e.g. Eq. (7), where the “interaction” term in the self energy is determined by the ε_k 's, the fourier transforms of the hopping matrix elements. A surprisingly low characteristic temperature scale^{20,31} emerges from the strong correlations, above which the resistivity crosses over from Fermi liquid type i.e. $\rho \sim T^2$ behavior, to an almost linear type i.e. $\rho \sim T$ behavior.

Here we address the effect of strain on the resistivity via its change of the hopping amplitudes. At a qualitative level, strain influences the hopping amplitude by changing the overlap between nearby orbitals, a small strain can be parametrized through a single variable α as discussed in Eq. (13). We can estimate this single parameter by computing (or measuring) other physical variables which also change with strain. For this purpose we have identified two experimentally accessible variables. Firstly we study the integrated weight of the anisotropic electrical optical conductivity, i.e., the f-sum rule weight, accessible in optical experiments^{26,27}. Secondly we study the local density of states (LDOS), measurable through scanning tunneling microscopy (STM)²¹⁻²⁵. The f-sum rule weight in tight binding systems is related to the expectation of the kinetic energy, or hopping, and can be obtained from the Greens function. The LDOS can be calculated from the local Greens function easily.

From the above we argue that strain effects could provide a test of the underlying mechanism for resistivity within the ECFL theory to include strain dependence. Experiments probing these strain effects are likely in the near future, thus enabling an important test of the theory.

The plan of the paper is as follows: In Sec. II (A) we summarize the second order ECFL equations and the corresponding Green's functions and self-energies. (B) We describe how to convert the lattice constants and hopping parameters for system under strain. (C) We outline the parameters for the program. In Sec. III, we present the calculation of and results for (A) the resistivity, (B) the kinetic energy, and (C) the LDOS and their associated susceptibilities with respect to strain. We provide a brief

summary and discussion of our results and future work in Sec. IV.

II. METHODS & PARAMETERS

A. The ECFL Equations

In this section, we briefly introduce the ECFL equations for the t - t' - J model. More details can be found in Ref. [11,28,29,32]. In the ECFL theory,²⁸ the one-electron Green's function in momentum space is characterized as a product of an auxiliary Green's function \mathbf{g} and a caparison function $\tilde{\mu}$:

$$\mathcal{G}(k) = \mathbf{g}(k) \times \tilde{\mu}(k) \quad (1)$$

where $k \equiv (\mathbf{k}, i\omega_n)$ and $\omega_n = (2n+1)\pi k_B T$ is the Fermionic Matsubara frequency. The auxiliary $\mathbf{g}(k)$ plays the role of a Fermi-liquid type Green's function whose asymptotic behavior is $1/\omega$ as $\omega \rightarrow \infty$, and $\tilde{\mu}$ is an adaptive spectral weight that mediates between two conflicting requirements²⁹: (1) the high frequency behavior of the non-canonical fermions and (2) the Luttinger-Ward volume theorem at low frequencies.

The equation of the Green's function for t - t' - J model can be symbolically written as³²

$$\left(\mathbf{g}_0^{-1} - \hat{X} - Y_1 \right) \cdot \mathcal{G} = \delta (\mathbf{1} - \gamma). \quad (2)$$

where \hat{X} represents a functional derivative and Y_1 stands for the \mathcal{G} convoluted with hopping and interaction. They are in analogy with the left side in the Schwinger-Dyson equation for Hubbard model: $(\mathbf{g}_0^{-1} - U\delta/\delta\mathcal{V} - UG) \cdot G = \delta \mathbf{1}$. On the right side of Eq. (2), γ is proportional to a local \mathcal{G} and originates from the non-canonical algebra of creation and annihilation operators. The non-canonical nature and the lack of an obvious small parameter for expansion are the main difficulties to solve this equation.

To tackle these difficulties, the ECFL theory rewrites Eq. (2) into

$$\left(\mathbf{g}_0^{-1} - \lambda\hat{X} - \lambda Y_1 \right) \cdot \mathcal{G} = \delta (\mathbf{1} - \lambda\gamma). \quad (3)$$

where $\lambda \in [0, 1]$ interpolates from non-interacting to fulling interacting system. Then we expand Eq. (3) systematically with respect to λ up to a finite order and at the end setting $\lambda = 1$ to recover the full t - t' - J physics. The introduction of λ bound to $[0, 1]$ in ECFL makes it possible that a low-order expansion could be enough to describe low-energy excitation in a large region of doping. This argument has been justified in one⁴⁰ and infinite¹¹ dimensions by benchmarking against exact numerical techniques and in two^{31,32} dimensions by comparing well with experiments.

In the following, we use the minimal version of second order (in λ) ECFL equations³², setting the super-exchange term to $J = 0$, which is equivalent to the

infinite- U Hubbard model:

$$\begin{aligned} \tilde{\mu}(k) &= 1 - \lambda \frac{n}{2} + \lambda \psi(k) \\ \mathbf{g}^{-1}(k) &= i\omega_n - (\epsilon_{\mathbf{k}} - \boldsymbol{\mu}) + \lambda \frac{n}{2} \epsilon_{\mathbf{k}} - \lambda \phi(k) \end{aligned} \quad (4)$$

where $\boldsymbol{\mu}$ is the standard chemical potential. The non-canonical Green's function features two self-energy terms: the usual Dyson-like self-energy denoted $\phi(k)$ in the denominator and a second self-energy in the numerator $\psi(k)$. The self-energy $\phi(k)$ can conveniently be decomposed as follows: $\phi(k) = \chi(k) + \epsilon'_{\mathbf{k}} \psi(k)$ where $\chi(k)$ denotes a self-energy part, $\epsilon'_{\mathbf{k}} = \epsilon_{\mathbf{k}} - u_0/2$ and $\psi(k)$ the second self-energy. Here u_0 acts as a Lagrange multiplier, enforcing the shift invariance^{28,29,32} of the t - t' - J model at every order of λ . The second order example is given in the discussion below Eq. (8). The expressions for these self-energies in the second order theory are given by

$$\psi(k) = - \sum_{pq} (\epsilon'_p + \epsilon'_q) \mathbf{g}(p) \mathbf{g}(q) \mathbf{g}(p+q+k) \quad (6)$$

and $\chi_0 + \lambda\chi_1$ with $\chi_0(k) = - \sum_{\mathbf{p}} \epsilon'_p g(p)$

$$\chi_1(k) = - \sum_{pq} (\epsilon'_p + \epsilon'_q) \epsilon'_{p+q-\mathbf{k}} \mathbf{g}(q) \mathbf{g}(p+q-k) \quad (7)$$

where $\sum_k \equiv \frac{k_B T}{N_s} \sum_{\mathbf{k}, \omega_n}$. By setting λ to 1, the resulting expressions for the second order equations are

$$\tilde{\mu}(k) = 1 - \frac{n}{2} + \psi(k) \quad (8)$$

$$\begin{aligned} \mathbf{g}^{-1}(k) &= i\omega_n - (\epsilon_{\mathbf{k}} - \boldsymbol{\mu}) + \frac{n}{2} \epsilon_{\mathbf{k}} - \chi_0(k) \\ &\quad - \chi_1(k) - \epsilon'_p \psi(k) \end{aligned} \quad (9)$$

We can verify that an arbitrary shift of $\epsilon_{\mathbf{k}} \rightarrow \epsilon_{\mathbf{k}} + c_0$ leaves the above expression invariant by shifting $\boldsymbol{\mu} \rightarrow \boldsymbol{\mu} + c_0$ and $u_0 \rightarrow u_0 + 2c_0$. In this sense, we may take u_0 as a second chemical potential. Here, n denotes the particle density from which we can determine the two chemical potentials μ and u_0 by satisfying the following number sum rules

$$\sum_k \mathbf{g}(k) e^{i\omega_n 0^+} = \frac{n}{2} = \sum_k \mathcal{G}(k) e^{i\omega_n 0^+}. \quad (10)$$

We find the spectral function $\rho_{\mathcal{G}}(k) = -1/\pi \Im m \mathcal{G}(k)$ by analytically continuing (i.e. $i\omega_n \rightarrow \omega + i\eta$) and by solving Eq. (1) and Eqs. (6-10) recursively. We remind the reader that the spectral function $\rho_{\mathcal{G}}(k)$ is referred to in most experimental literature by the symbol $A(\mathbf{k}, \omega)$. We can recover the interacting Green's function from $\rho_{\mathcal{G}}$ using

$$\mathcal{G}(\mathbf{k}, i\omega_n) = \int_{-\infty}^{\infty} \frac{\rho_{\mathcal{G}}(\mathbf{k}, \nu)}{i\omega_n - \nu} d\nu. \quad (11)$$

B. Strain effects on hopping

§Converting lattice constant changes to hopping changes: We are working with the t-t'-J model in two dimensions, and the parameters amenable to strain-variation are

$$t_x, t_y, t', \quad (12)$$

where t_x and t_y refer to nearest neighbor hops along x and y axes, and t' is the second neighbor hopping matrix element on the square lattice. We start with the tetragonal symmetry case where there are just two parameters:

$$t_x = t_y = t, \quad t'$$

The t-t'-J model describes hopping of electrons between coppers in the 2-d plane. At the level of a single bond between two coppers, any hopping $t(R)$ for a bond with length R can be represented by³³

$$t(R) \sim \frac{A}{R^\alpha} \quad (13)$$

where A is a constant. In the simplest cases, the exponent α is given by the angular momentum l_1, l_2 of the relevant atomic shells of the two atoms by the formula

$$\alpha = l_1 + l_2 + 1. \quad (14)$$

Thus for two copper atoms $l_1 = l_2 = 2$ and hence we might expect

$$\alpha \sim 5, \quad (15)$$

whereas for copper oxygen bonds $l_1 = 2, l_2 = 1$, therefore

$$\alpha \sim 3. \quad (16)$$

For the effective single band description of the cuprate materials, it is not entirely clear what value of α is most appropriate. Comparisons with experiments might be the best way to decide on this question, when the results become available. Until then we can bypass this issue by presenting the theoretical results in terms of $\frac{\delta t}{t}$ rather than the strain itself. Towards this end Eq. (13) is a very useful result. We rewrite it as

$$\frac{\delta t(R)}{t(R)} = -\alpha \frac{\delta R}{R}, \quad (17)$$

thus enabling us to convert a change of the lattice constant to that of the corresponding hopping, using only the value of t and α . Throughout this paper we will refer to $\delta t/t$ as the hopping strain in order to distinguish it from the conventional strain, $\delta R/R$. The hopping strain will always refer to the strain along the x axis unless otherwise noted.

§Geometrical aspects of the strain variation

Our calculation studies a few variations of parameters. We start with an undistorted tetragonal system

at $t \sim 5220\text{K}$, and vary t' to capture both electron doped ($t' > 0$) and hole doped ($t' < 0$) cuprates. For a general orthorhombic case with lattice constants a, b , the three distances of interest (two sets of nearest neighbors and one set of second neighbors) are

$$a, b, \rho = \sqrt{a^2 + b^2}. \quad (18)$$

For the tetragonal case we set $a = b = a_0, \rho = \sqrt{2}a_0$, where we refer to the undistorted lattice parameter as a_0 . We next study the effect of stretching ($\delta a > 0$) or compressing ($\delta a < 0$) the x -axis, leaving the y -axis lattice constant unchanged. The changes in the lattice constants then read as

$$a \rightarrow a_0 + \delta a; \quad b \rightarrow a_0; \quad \rho \rightarrow \sqrt{2}a_0 + \frac{\delta a}{\sqrt{2}}. \quad (19)$$

We denote the strain in the x-direction as

$$\epsilon_{xx} = \epsilon = \frac{\delta a}{a_0}. \quad (20)$$

In terms of the strain, we can rewrite the distances to neighbors as

$$a = a_0(1 + \epsilon), \quad b = a_0, \quad \rho = \sqrt{2}a_0 \left(1 + \frac{\epsilon}{2}\right). \quad (21)$$

The single particle (tight binding) energies for the distorted lattice are given by

$$\epsilon_k = -2t_x \cos(k_x a) - 2t_y \cos(k_y b) - 4t_d \cos(k_x a) \cos(k_y b). \quad (22)$$

In terms of the band parameters of the unstrained system, t and t' , we can write the anisotropic band parameters as

$$\begin{aligned} t_x &= (1 - \alpha \epsilon) t \\ t_y &= t \\ t_d &= (1 - \alpha \frac{\epsilon}{2}) t', \end{aligned} \quad (23)$$

where the factor of $\frac{1}{2}$ for t_d comes about due to a shorter stretching of ρ as in Eq. (21).

C. Parameters in the program

The model considered applies to several classes of materials, such as the cuprates, the sodium cobaltates and presumably also to the iron arsenide superconductors. We shall restrict our discussion to the cuprates where the parameters are fairly well agreed upon in the community^{34,35}.

In this calculation, we set $t = 1$ as our energy scale and we allow t'/t to vary between -0.4 and 0.4 . The hopping strain $\delta t/t$ is varied from -0.15 to 0.15 . We can convert to physical units by equating $t = 0.45\text{eV}$, and hence the band width $W = 8t = 3.6\text{eV}$. We focus on two particle densities, optimal doping $\delta = (1 - n) = 0.15$

and overdoped case $\delta = 0.20$. Here δ the hole doping is related to the particle density $n = 1 - \delta$. The temperature is range is set $T \in [37, 450]\text{K}$ except at $t' = 0.2$ and $n = 0.80$. Lower temperatures than this lie outside the range of convergence for the current scheme. For the interacting system we solve the ECFL equations (6-10) iteratively on a frequency grid of $N_\omega = 2^{14}$ and a lattice $L \times L$ with $L = 61, 79, 135$ where N_ω is the dimensions of the frequency grid and L is number of elements in the lattice for each direction. We primarily use an $L > 61$ for $t' > 0$ at low temperatures (i.e. $T < 100\text{K}$) in order to get sufficient resolution to converge electrical resistivity calculation. The need for a high resolution lattice at low temperatures is a product of the spectral function which features higher, sharper peaks for $t' > 0$, to which the resistivity calculation is sensitive³². For the non-interacting system we compute LDOS using a system of size $N_\omega = 2^{12}$ and $L = 271$.

III. SELECTION OF RESULTS

Here we present the effects of strain on electrical resistivity, kinetic energy and LDOS and their associated susceptibilities in response to a compressive ($\delta t/t > 0$) and tensile ($\delta t/t < 0$) hopping strain.

A. Resistivity for an x-axis strain:

We now study the response of electrical resistivity characterized by electron-electron scattering³² in the presence of a strain. We use the bubble approximation, factoring the current correlator as $\langle J(t)J(0) \rangle \sim \sum_{\mathbf{k}} \gamma_{\mathbf{k}}^2 \mathcal{G}(k)$ with a suitable vertices $\gamma_{\mathbf{k}}$ and dressed Green's function to compute the components of dimensionless resistivity tensor, ρ_{ij} . We shall calculate and quote the following objects:

- $\rho'_{xx}(n, T)$ is the strained version of resistivity along x-axis.
- $\rho'_{yy}(n, T)$ is the strained version of resistivity along y-axis.
- ρ_{xx} without a prime refers to the tetragonal result, which is the same as ρ_{yy} .
- We present XX component variations

$$(\rho'_{xx} - \rho_{xx})/(\rho_{xx}\delta t/t) \text{ vs } T$$

- We present YY component variations

$$(\rho'_{yy} - \rho_{yy})/(\rho_{yy}\delta t/t) \text{ vs } T$$

- We present A_{1g} symmetry variations

$$\frac{\rho'_{xx} + \rho'_{yy} - 2\rho_{xx}}{2\rho_{xx}\delta t/t} \text{ vs } T$$

- We present B_{1g} symmetry variations

$$(\rho'_{xx} - \rho'_{yy})/(\rho_{xx}\delta t/t) \text{ vs } T$$

We noted that $\rho'_{xx} + \rho'_{yy}$ corresponds to the A_{1g} irreducible representation (irrep) and $\rho'_{xx} - \rho'_{yy}$ corresponds to the B_{1g} irrep of the D_{4h} point group³⁶⁻³⁹.

§Computation of the anisotropic resistivity

To find the anisotropic resistivity, we compute the dimensionless conductivity³² for the anisotropic case

$$\sigma_{xx} = \langle \Upsilon_{\mathbf{k}} (\hbar v_{\mathbf{k}}^x)^2 / (ab) \rangle_{\mathbf{k}}, \quad (24)$$

$$\sigma_{yy} = \langle \Upsilon_{\mathbf{k}} (\hbar v_{\mathbf{k}}^y)^2 / (ab) \rangle_{\mathbf{k}} \quad (25)$$

where $\langle A \rangle_{\mathbf{k}} = \frac{1}{N_s} \sum_{\mathbf{k}} A$, $N_s = L \times L$ and

$$\Upsilon_{\mathbf{k}} = (2\pi)^2 \int_{-\infty}^{\infty} d\omega (-\partial f / \partial \omega) \rho_G^2(k) \quad (26)$$

where $f(\omega) \equiv 1/(1 + \exp(\beta\omega))$ is the Fermi function, $\rho_G(k)$ is the spectral function from second order ECFL theory and $v_{\mathbf{k}}^x, v_{\mathbf{k}}^y$ are the bare vertices which are defined as

$$v_{\mathbf{k}}^x = \frac{1}{\hbar} \frac{\partial \epsilon_{\mathbf{k}}}{\partial k_x} = \frac{a}{\hbar} \frac{\partial \epsilon_{\mathbf{k}}}{\partial k_1}, \quad (27)$$

$$v_{\mathbf{k}}^y = \frac{1}{\hbar} \frac{\partial \epsilon_{\mathbf{k}}}{\partial k_y} = \frac{b}{\hbar} \frac{\partial \epsilon_{\mathbf{k}}}{\partial k_2} \quad (28)$$

where $k_1 = k_x a$ and $k_2 = k_y b$ denote the dimensionless momentum components. Inserting the dimensionless momenta into Eq. (25), we obtain

$$\sigma_{xx} = \left\langle \Upsilon_{\mathbf{k}} \left(\frac{d\epsilon_{\mathbf{k}}}{dk_1} \right)^2 (a/b) \right\rangle_{\mathbf{k}}, \quad (29)$$

$$\sigma_{yy} = \left\langle \Upsilon_{\mathbf{k}} \left(\frac{d\epsilon_{\mathbf{k}}}{dk_2} \right)^2 (b/a) \right\rangle_{\mathbf{k}} \quad (30)$$

for the dimensionless conductivity. The corresponding dimensionless resistivities are $\rho_{xx} = 1/\sigma_{xx}$ and $\rho_{yy} = 1/\sigma_{yy}$. The electrical resistivity can be converted to physical units as follows: $\rho_{physical, \alpha} = \rho_{\alpha} \times \rho_0$ where $\rho_0 = c_0 \hbar / e^2 \sim 1.171 \text{m}\Omega\text{cm}$, and $\alpha = xx$ describes the longitudinal (parallel to strain) resistivity and yy describes the transverse (perpendicular to strain) resistivity. Here $c_0 \sim 6.645 \text{\AA}$ is the typical separation between parallel planes⁴¹.

1. The raw resistivities

In our recent work³¹, a significant finding was the t' dependence of the curvature of resistivity versus temperature curve. Here we focus on the effects that hopping strain, $\delta t/t$, has on resistivity. In particular, in Fig. 1, we study the anisotropy of the raw dimensionless resistivity over a broad range of temperatures for two representative densities: over-doped ($n = 0.80$) and optimal ($n = 0.85$)

density. It displays the longitudinal resistivity ρ'_{xx} (solid) and the transverse resistivity ρ'_{yy} (dashed) for a compressive strain (red) and tensile strain (blue) in comparison to the unstrained tetragonal system (green). We observe that longitudinal resistivity under a compressive strain ($\delta t/t > 0$) is enhanced and conversely, under a tensile strain ($\delta t/t < 0$) it is reduced across the displayed temperatures range and for all t' . The response for transverse resistivity is similar except the sign of change is t' dependent, and there is a reduction in the magnitude of the change. An interesting new feature lies in the t' dependence, we note that magnitude of the change in transverse resistivity is t' dependent where for $t' = 0.2t$ it is unchanged for all strains, and hence, by measuring the transverse resistivity we can determine the sensitivity of the system to second neighbor interactions.

Consistent with previous findings, we observe that the curvature persists under strain, i.e., the curvature changes from positive (concave up like $+T^2$) to negative (convex up like $-T^2$) as t'/t is varied upward. Recall that strain is effectively a small change in the hopping parameter, so we ought to expect strain to have a similar impact on the curvature. Phenomenologically, varying t' signals a change in the effective Fermi temperature scale T_{FL} where for $T < T_{FL}$ the system is in the Fermi liquid regime, $\rho \propto T^2$ and hence has a positive curvature. Moreover, as we decrease t' from positive to negative, we suppress the Fermi liquid temperature regime into a smaller temperature regime at low temperatures which is usually hidden by the superconducting state. The observed negative curvature is indicative of an extended crossover region from Fermi-liquid regime to the strange-metal regime for $T > T_{FL}$ with linear behavior. The following relation is useful to express the crossover regime for high enough hole doping

$$\rho \sim C \frac{T^2}{T_{FL} + T} \quad (31)$$

where C is a constant that defines the slope of linear regime and T_{FL} marks the crossover. For $t' = -0.2t$, we find the following: We find that a compressive (tensile) strain extends the Fermi-liquid regime for the longitudinal (transverse) resistivity, and flipping the strain reduces the Fermi-liquid regime. The difference in magnitude of the response between the longitudinal and transverse resistivity under compression is characterized by the relation $t_d/t_x > t_d/t_y$ and hence the longitudinal resistivity is more Fermi-liquid-like. Conversely, we see that a compressive strain reduces the Fermi-liquid temperature scale for the transverse resistivity sending the ρ_{yy} - T curve to the linear regime more quickly, and enlarges the resistivity at high temperatures indicating an enhanced linear constant, C . Although not shown in Fig. 1, we also note that increasing the magnitude of the compressive strain extends the Fermi-liquid regime of the longitudinal resistivity, all of which is consistent with the above relation.

2. Strain-Resistivity susceptibilities for A_{1g} irrep

In this section we shall examine the normalized susceptibility, i.e., the response function for the resistivity in the A_{1g} irrep,

$$\chi_{A_{1g}} \equiv -\left(\frac{\rho'_{xx} + \rho'_{yy} - 2\rho_{xx}}{2\rho_{xx}}\right) / \left(\frac{\delta t}{t}\right). \quad (32)$$

It is also useful to record the unnormalized susceptibility

$$\chi_{A_{1g}}^{(u)} \equiv -\left(\rho'_{xx} + \rho'_{yy} - 2\rho_{xx}\right) / \left(\frac{\delta t}{t}\right). \quad (33)$$

In Figs. 2 and 3 we present the unnormalized [(a),(c),(e),(g)] and normalized [(b),(d),(f),(h)] response functions at two representative densities: $n = 0.80$, $n = 0.85$, respectively, for various t' and $\delta t/t$. The resistivity for A_{1g} irrep is defined as the sum, $\rho_{xx} + \rho_{yy}$, which acts as a center of mass coordinate and the susceptibility highlights the shift in this coordinates as result of strain. Since the resistivity vanishes as $T \rightarrow 0$, we note that the normalized susceptibility is enhanced at low- T . As a result of the anisotropy in hopping parameters, t_d/t_x , t_d/t_y , there is slight asymmetry between the response function to a compressive and tensile strain of the of similar magnitude.

From Figs. 2 and 3 we see that at $T \gtrsim 100\text{K}$ and for hole doping, i.e. $t' \leq 0$, the normalized susceptibilities become independent of the strain, and hence the response is in the linear regime. The non-linear response at lower T is interesting and potentially observable in experiments with varying strain.

On the other hand for electron doping, i.e. $t' > 0$, we see a strongly non-linear behavior even at high T . Its origin is the extended Fermi-liquid regime in this case. Summarizing, we find that the early departure from Fermi liquid behavior into a strange metallic behavior in the hole doping favors a linear response above 100K. Conversely we expect to see non-linearity extending to much higher T 's.

3. Strain-Resistivity susceptibilities with B_{1g} irrep

In this section, we shall examine the response function for the B_{1g} irrep defined as

$$\chi_{B_{1g}} \equiv -\left(\frac{\rho'_{xx} - \rho'_{yy}}{\rho_{xx}}\right) / \left(\frac{\delta t}{t}\right), \quad (34)$$

$$\chi_{B_{1g}}^{(u)} \equiv -\left(\rho'_{xx} - \rho'_{yy}\right) / \left(\frac{\delta t}{t}\right). \quad (35)$$

In Eqs. (32)-(37) the strain $\delta t/t$ is taken to be small but non-zero. For non-zero values of strain the non-linear components of response are picked up. These are also of interest, and we comment on them below

In Figs. 4 and 5, we display the unnormalized [(a),(c),(e),(g)] and normalized [(b),(d),(f),(h)] response

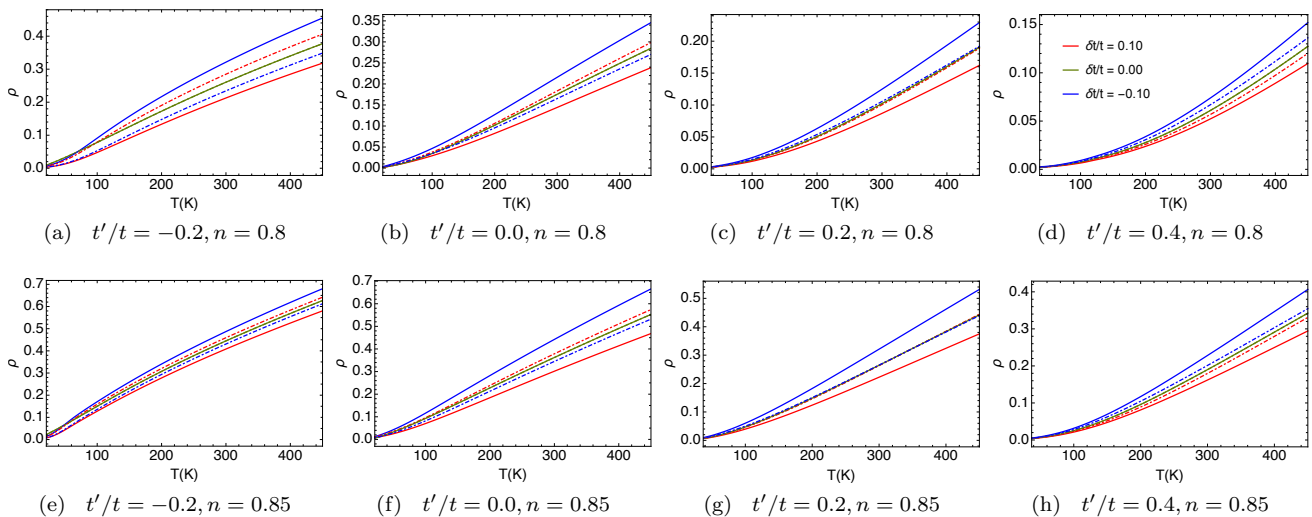


FIG. 1: The longitudinal and transverse resistivities, ρ'_{xx} (solid) and ρ'_{yy} (dashed) respectively, versus temperature at filling $n = 0.8, 0.85$ for various t' , and at a representative compressive and tensile strains, $\delta t/t$. All figures share the legend. The resistivity in physical units can be found by $\rho_{physical} = \rho \times \rho_0$, where $\rho_0 = c_0 h/e^2 \sim 1.17 \text{m}\Omega \text{cm}$.

functions at two representative densities: $n = 0.80$, $n = 0.85$, respectively, for various t' and $\delta t/t$. The resistivity for B_{1g} irrep is defined as the difference, $\rho_{xx} - \rho_{yy}$, which plays the role the relative coordinate and the susceptibility characterizes the shift in this coordinates as result of strain. In the unstrained system the $\rho_{xx} = \rho_{yy}$, and hence the B_{1g} irrep vanishes for the unstressed system. Since the resistivity vanishes as the $T \rightarrow 0$, we note that the normalized susceptibility is enhanced at low- T .

Now let us discuss the t' dependence of the susceptibilities. Similar to the $\rho - T$ curve, the curvature of the unnormalized response function goes from positive to negative as t' increases from negative to positive. At high- T we see that the response function increases monotonically with strain, that is, for all t' the response function is more sensitive to a tensile strain than to a compressive strain. This asymmetry is related to the difference in anisotropic hopping parameters, $t_d/t_x - t_d/t_y$ which leads a faster divergence between ‘strange metal’ regimes of the anisotropic resistivities for tensile strains than compressive strain. Recall that an increase in t' as a result of hopping strain enhances the Fermi-liquid like behavior. At high- T , the sensitivity of the response function to follows from the anisotropic hopping parameters, e.g., under a compressive strain the Fermi-liquid regime is extended for the longitudinal resistivity, whereas for transverse resistivity the Fermi-liquid regime is rapidly reduced as result of the anisotropy the hopping parameters and vice versus for a tensile strain. This relation to T_{FL} produces a response function that is more sensitive to a tensile strain than at high- T for all t' . At low- T , however, the response function with respect to strain is t' dependent. This strange behavior at low- T primarily comes from spectral function Eq. (25). We also note that for a given strain the sensitivity increases as t' decreases. This

follows from a reduced Fermi-liquid temperature scale with a steeper linear ‘strange metal’ regime and a more rapid divergence between the longitudinal and transverse resistivity resulting in a more sensitive response function at high temperatures.

Now let us discuss the linearity or otherwise of the response function with respect to the strain, as seen in Figs. 4 and 5. The response function displays linearity with strain in the ‘strange metal’ temperature regime, but is quadratic in the Fermi liquid regime. This is indicated by the evenly spaced $\rho - T$ curve for different $\delta t/t$. As t' is increases, that is as T_{FL} increase, the response function becomes increasingly uniform across the temperature range.

4. Strain-Resistivity susceptibilities for anisotropic resistivity

In this section, we shall examine the response function for the longitudinal and transverse resistivity defined as

$$\chi_{XX} \equiv -\left(\frac{\rho'_{xx} - \rho_{xx}}{\rho_{xx}}\right) / \left(\frac{\delta t}{t}\right), \quad (36)$$

$$\chi_{YY} \equiv -\left(\frac{\rho'_{yy} - \rho_{yy}}{\rho_{yy}}\right) / \left(\frac{\delta t}{t}\right), \quad (37)$$

respectively.

In Figs. 6 and 7, we show the strain-resistivity response function for the longitudinal [(a),(c),(e),(g)] and transverse [(b),(d),(f),(h)] response functions at two representative densities: $n = 0.80$, $n = 0.85$, respectively, for various t' and $\delta t/t$. First we study the response function for the longitudinal resistivity. In comparing the two representative densities, we observe a slight change in

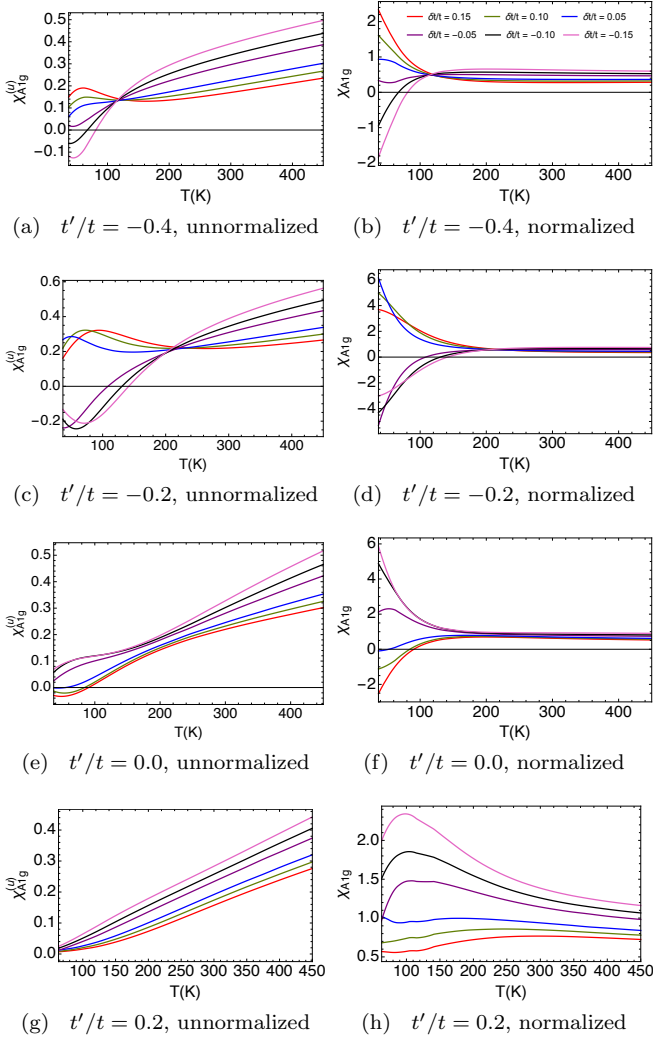


FIG. 2: The unnormalized and normalized strain-resistivity susceptibilities from Eq. (33) and Eq. (32) versus temperature for the A_{1g} irrep at filling $n = 0.80$. All the figures share a legend where we vary $\delta t/t$.

linearity of the response function as a result of increased correlations. Examining the T dependence for $t' = -0.2t$, we see that there is a non-linearity at low temperatures; This low- T dependence comes from the self-energies in the presence of strain. At high- T the response function is weakly second order due to the slight difference in the linear ‘strange metal’ regime after the crossover. As we vary t' to more positive value (more Fermi-liquid-like behavior) the response function is less sensitive at low- T . Conversely, if we shift t' to more negative values, the sensitivity increases at low- T . This difference in sensitivity, may be explained by examining the anisotropic hopping parameters, $t_d/t_x, t_d/t_y$, which are more sensitive for $t' < 0$. We observe that systems with a smaller T_{FL} are more sensitive to strain at low temperatures. A compressive (tensile) strain increases (decreases) T_{FL} , which marks a gradual crossover to the linear ‘strange

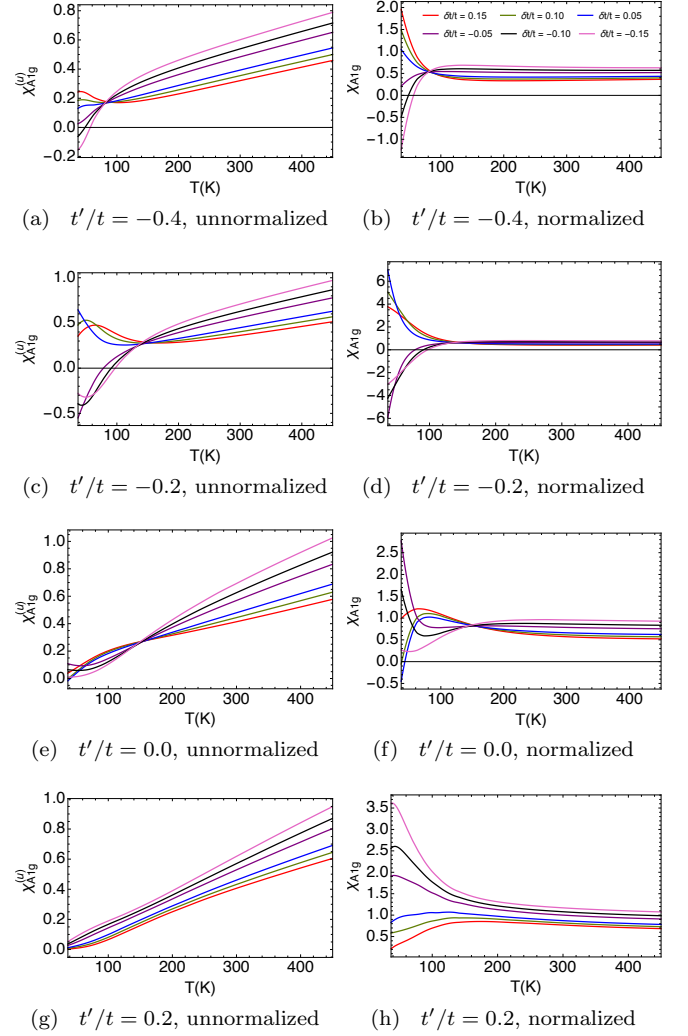


FIG. 3: The unnormalized and normalized strain-resistivity susceptibilities from Eq. (33) and Eq. (32) versus T for the A_{1g} irreducible representations at filling $n = 0.85$. All the figures share a legend.

metal’ region. We also note a slight asymmetry in the response between tensile and compressive strain.

In comparing the longitudinal and transverse response functions we see that the line shapes are similar for each t' , except that the transverse response has stronger linearity at high- T . Here, we note the response to a compressive strain and tensile strain is t' dependent. For $t' < 0$, a compressive (tensile) strain lowers (raises) T_{FL} followed by a rapid (gradual) crossover to the linear ‘strange metal’ regime. For $t' > 0$, a compressive (tensile) strain raises (lowers) the T_{FL} , but is followed by a more gradual (rapid) crossover to the Fermi-liquid regime. We surmise that is different at $t' > 0$ exist for two reasons (1) the higher the Fermi-liquid temperature is more robust and (2) that the anisotropic hopping parameters $t_d/t_x, t_d/t_y$ are less sensitive for $t' > 0$. We note that the linearity of the response function at high- T

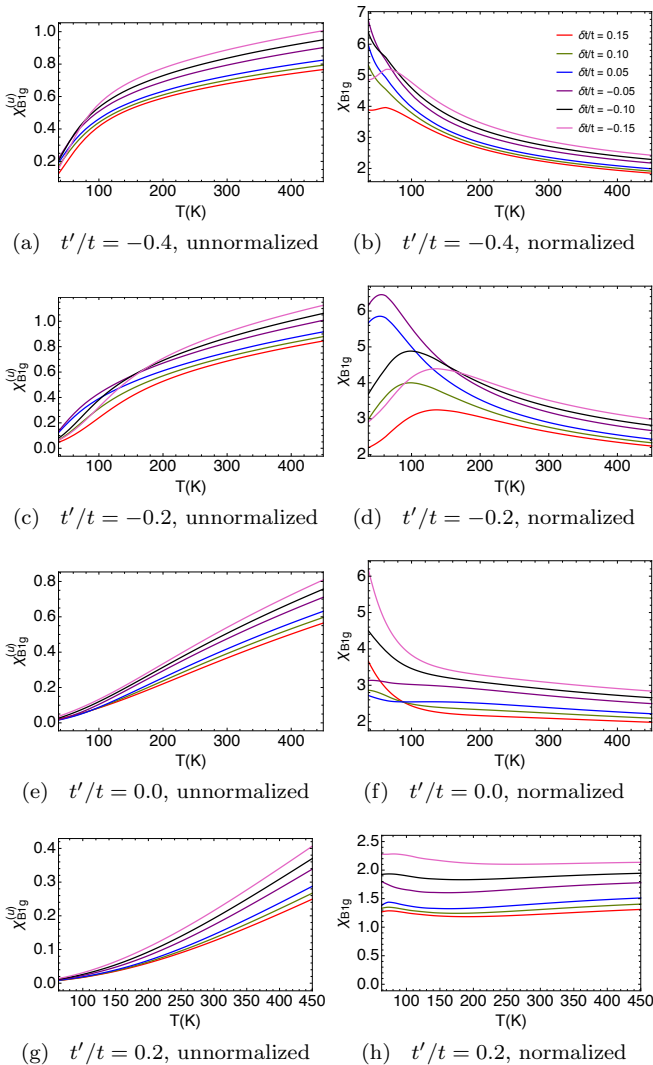


FIG. 4: The unnormalized (Eq. (35)) and normalized (Eq. (34)) strain-resistivity susceptibilities versus T for B_{1g} irrep at filling $n = 0.80$ at various t' and $\delta t/t$. All figures share a legend.

is due the smaller deviation from the unstrained system.

5. Susceptibilities versus strain

In Fig. 8, we display the response function versus strain for A_{1g} , B_{1g} , XX , and YY at $t' = -0.2t$ and $n = 0.85$ for various $\delta t/t$ at four representative temperatures. We first look at the response function for A_{1g} which we note is a linear response function when the line is horizontal. Here the response function becomes linear as we warm the system. The presence of a slope in the curve is indicative of a second order term in the response function, e.g., the curve in panel (d) at $T = 104\text{K}$ is linear nowhere. At low- T the response function displays non-linear behavior. In panels (a), (c) and (d) there is a wave-like

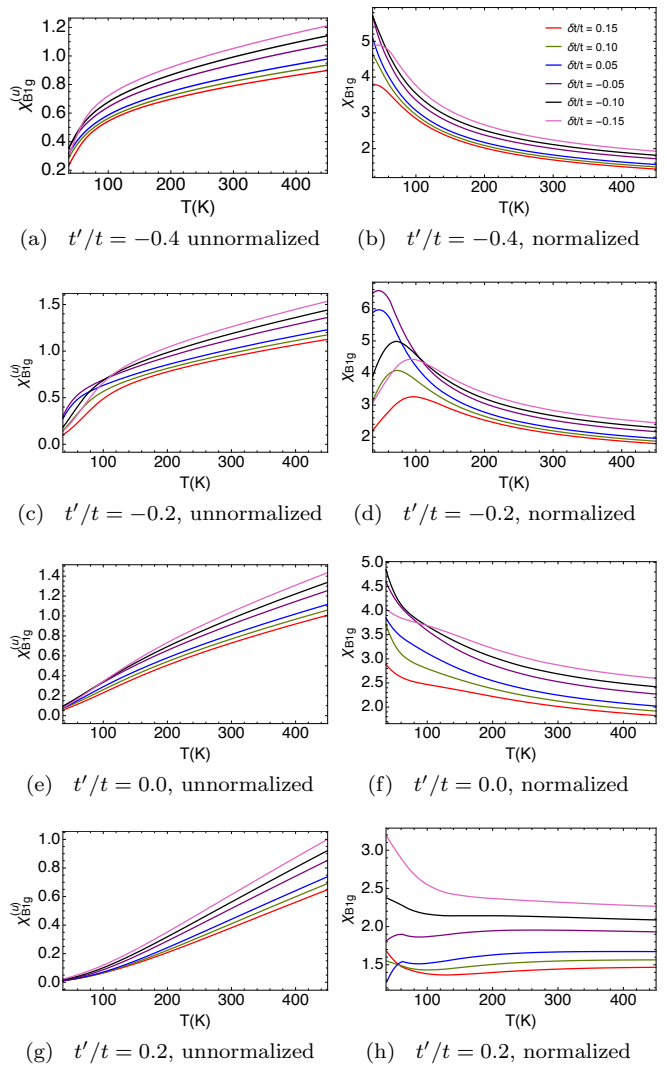


FIG. 5: The unnormalized (Eq. (35)) and normalized (Eq. (34)) strain-resistivity susceptibilities versus T for the B_{1g} irrep at filling $n = 0.85$ at various t' and $\delta t/t$. All figures share the legend.

oscillation which indicates the presence of higher order terms. In panel (b) we observe that response function is nearly symmetric with respect to compressive and tensile strain; however, there is a slightly increased sensitivity to tensile strain.

B. Kinetic Energy for an x-axis strain

In this section we explore the anisotropy of the kinetic energy for an ECFL under a strain along the x-axis. Since the anisotropic kinetic energy can be related to measurements of the optical conductivity using the f-sum rule on the t - t' - J model, this makes it an another interesting observable to explore.

The total kinetic energy for a system under strain is

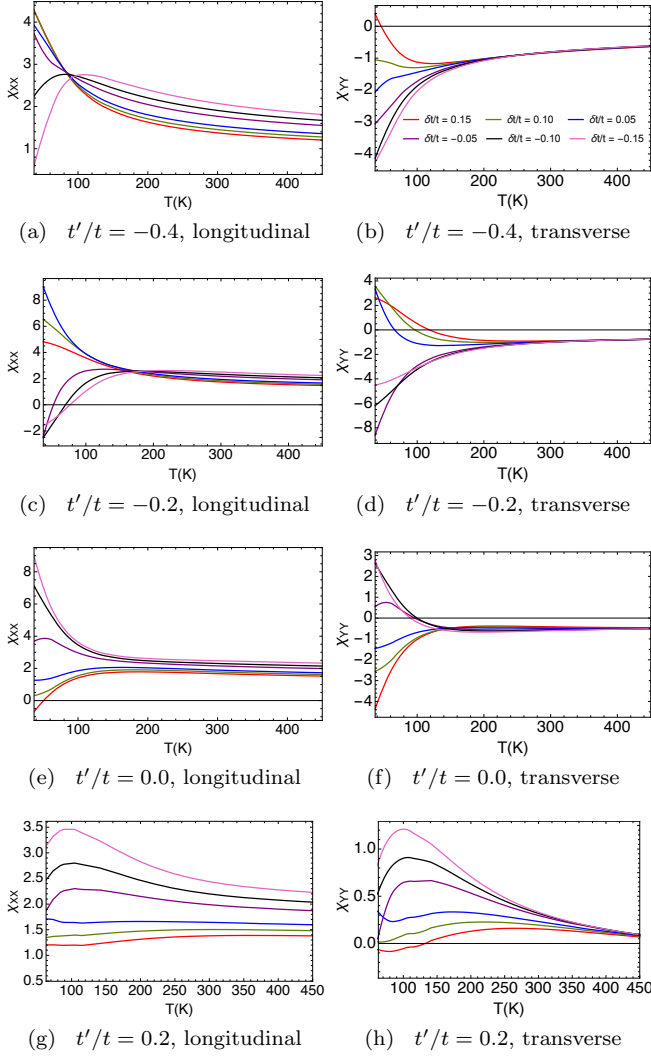


FIG. 6: The longitudinal (Eq. (36)) and transverse (Eq. (37)) strain-resistivity susceptibilities versus temperature at filling $n = 0.80$, for various t' and $\delta t/t$. All figures share a legend.

computed as

$$K_{\text{tot}} = \left\langle \int_{-\infty}^{\infty} \rho_{\mathcal{G}}(k) \epsilon_{\mathbf{k}} d\omega \right\rangle_{\mathbf{k}}. \quad (38)$$

This may be decomposed as follows:

$$K_{\text{tot}} = K_{xx} + K_{yy} + K_{xy}, \quad (39)$$

where K_{xy} is the kinetic energy along the diagonal of orthorhombic lattice and is isotropic for each diagonal. The longitudinal, transverse and diagonal kinetic energy

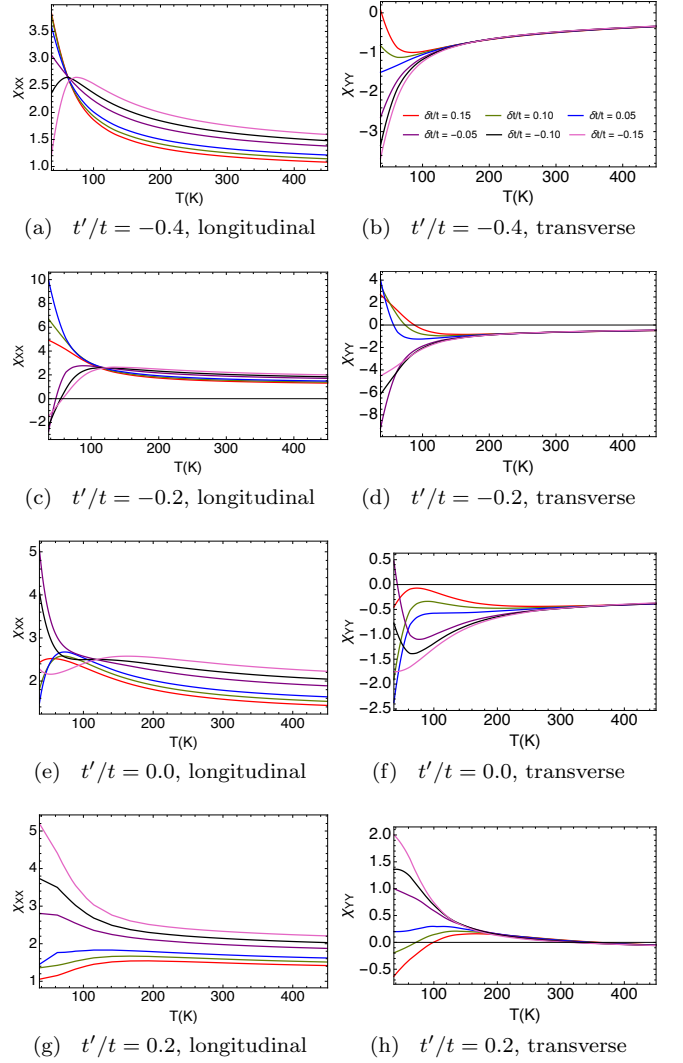


FIG. 7: The longitudinal (Eq. (36)) and transverse (Eq. (37)) strain-resistivity susceptibilities versus temperature at filling $n = 0.85$, for various t' and $\delta t/t$. All figures share a legend.

is given by

$$K_{xx} = \left\langle \int_{-\infty}^{\infty} \rho_{\mathcal{G}}(k) \epsilon_{k_x} \right\rangle_{\mathbf{k}} \quad (40)$$

$$K_{yy} = \left\langle \int_{-\infty}^{\infty} \rho_{\mathcal{G}}(k) \epsilon_{k_y} \right\rangle_{\mathbf{k}} \quad (41)$$

$$K_{xy} = \left\langle \int_{-\infty}^{\infty} \rho_{\mathcal{G}}(k) \epsilon_{k_{xy}} \right\rangle_{\mathbf{k}} \quad (42)$$

where

$$\epsilon_{\mathbf{k}_x} = -2t_x \cos(k_x a) \quad (43)$$

$$\epsilon_{\mathbf{k}_y} = -2t_y \cos(k_y b) \quad (44)$$

$$\epsilon_{\mathbf{k}_{xy}} = -4t_a \cos(k_x a) \cos(k_y b) \quad (45)$$

For the t - t' - J model, the anisotropic kinetic energies, denoted as K_{α} where $\alpha = xx$ and yy , is related to the

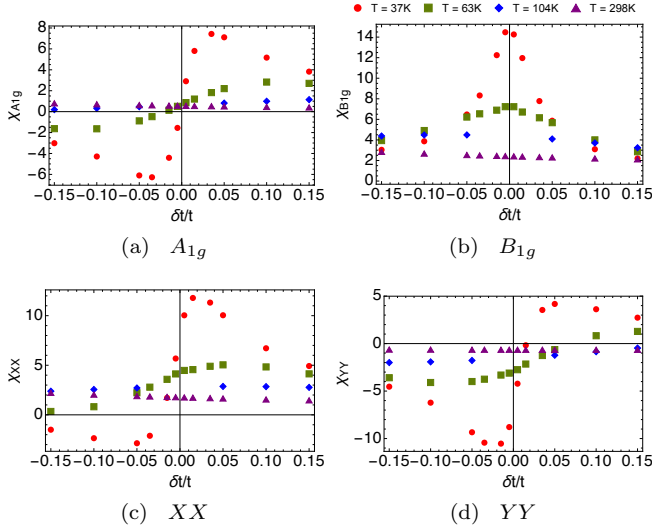


FIG. 8: The strain-resistivity susceptibilities four different representations as a function of strain $\delta t/t$ at filling $n = 0.85$ and $t'/t = -0.2$. (a) A_{1g} irrep, Eq. (32) (b) B_{1g} irrep, Eq. (34). (c) XX, longitudinal, Eq. (36). (d) YY, transverse, Eq. (37)

optical conductivity, σ_α , by the following sum rule

$$\Re \int_0^\infty \sigma_\alpha(\omega) d\omega = K_\alpha e^2, \quad (46)$$

where e is the electrical charge. $K_\alpha e^2$ sets the scale of the optical conductivity, i.e.,

$$\frac{1}{K_\alpha e^2} \Re \int_0^\infty \sigma_\alpha(\omega) d\omega = 1. \quad (47)$$

The optical conductivity in the DC limit, $\sigma_\alpha(0)$, is related the DC resistivity as follows: $\rho_\alpha(0) = 1/\sigma_\alpha(0)$. For the anisotropic kinetic energy we calculate and quote the following objects:

- $K'_{xx}(n, T)$, this is the strained version of longitudinal kinetic energy.
- $K'_{yy}(n, T)$ this is the strained version of transverse kinetic energy.
- We call K_{xx} without a prime as the tetragonal result. It is the same as K_{yy} .
- We present A_{1g} :

$$\frac{K'_{xx} + K'_{yy} - 2K_{xx}}{2K_{xx}\delta t/t} \text{ vs } T$$

- We present B_{1g} : $(K'_{xx} - K'_{yy})/(K_{xx}\delta t/t)$ vs T

1. Strain-kinetic-energy susceptibilities for the A_{1g} irrep

In this section, we shall examine the normalized and unnormalized kinetic energy response function for the A_{1g} irrep defined, respectively, as

$$M_{A_{1g}} \equiv -\left(\frac{K'_{xx} + K'_{yy} - 2K_{xx}}{2K_{xx}}\right) / \left(\frac{\delta t}{t}\right), \quad (48)$$

$$M_{A_{1g}}^{(u)} \equiv -\left(K'_{xx} + K'_{yy} - 2K_{xx}\right) / \left(\frac{\delta t}{t}\right). \quad (49)$$

In Fig. 9, we display the unnormalized and normalized strain-kinetic-energy susceptibilities versus temperature for the A_{1g} irrep at optimal density for various t' and $\delta t/t$. The A_{1g} irrep susceptibility signals a change in the sum of anisotropic kinetic energies, $K_{xx} + K_{yy}$. We observe that tensile strain uniformly reduces the total kinetic energy of the system and a compressive strain enhances it. Here, we will confine our attention to the normalized cases, Fig. 9(e)-(h). We observe that the response functions is non-linear throughout the displayed temperature range for all t' . The even spacing between curves at different hopping strains indicates that these are second order response functions. We also notice that the response function monotonically increases in absolute intensity as the system is warmed or the strain is increased from negative to positive.

2. Strain-Kinetic-Energy susceptibilities with B_{1g} symmetry

In this section, we shall examine the unnormalized and normalized response function of the kinetic energy for the B_{1g} irrep, respectively, defined as

$$M_{B_{1g}} \equiv -\left(\frac{K'_{xx} - K'_{yy}}{K_{xx}}\right) / \left(\frac{\delta t}{t}\right), \quad (50)$$

$$M_{B_{1g}}^{(u)} \equiv -\left(K'_{xx} - K'_{yy}\right) / \left(\frac{\delta t}{t}\right). \quad (51)$$

In Fig. 10, we display the unnormalized and normalized strain-kinetic-energy susceptibility versus T at optimal density ($n = 0.85$) at various t' for the B_{1g} irrep of the D_{4h} point group, which is characterized as the difference in the kinetic energies $K_{xx} - K_{yy}$ along the different direction of the distorted square lattice. The B_{1g} irrep indicates the presence of an anisotropy between the two directions. We note that shifting the density from over-doped to optimal has little effect on the response functions for $t' < 0$, except for a slight increase in the strength of the response for $t' \geq 0$ for that reason, we focus on the optimal density. First we see the character of the response function for the B_{1g} irrep is strongly t' dependent. For $t' = -0.4$, the response functions is nearly linear at all temperatures. We point out a curious feature for $t' = -0.2$ curve where at high- T the system is linear whereas at low- T the system is non-linear, but it nearly symmetric with respect to a compressive or tensile strain of similar magnitude. At high- T for all t' the

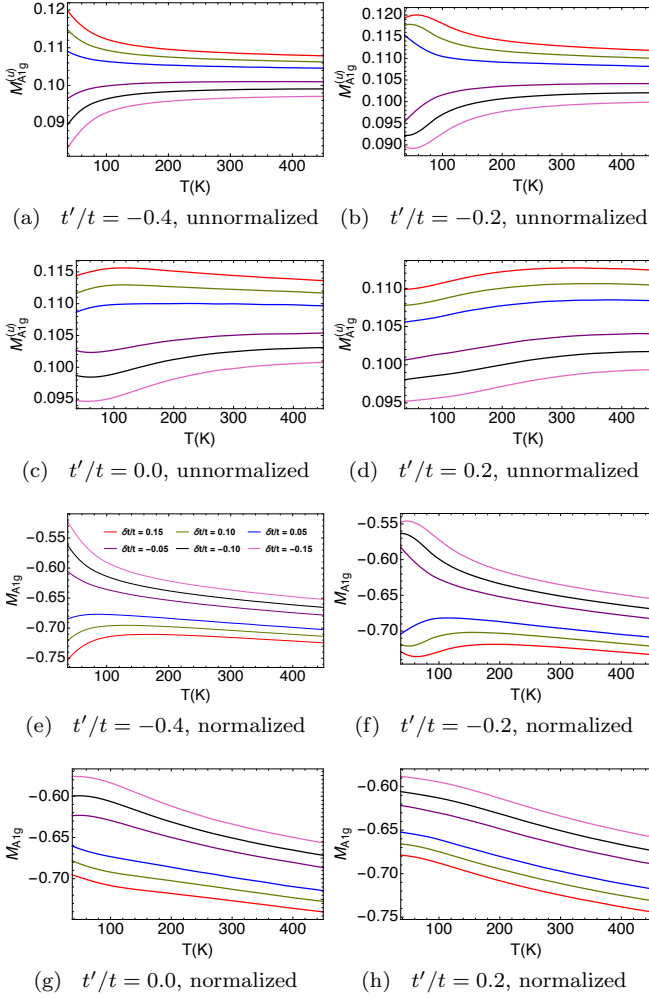


FIG. 9: The unnormalized and normalized strain-kinetic-energy susceptibilities for the A_{1g} irrep defined in Eq. (49) and Eq. (48) at filling $n = 0.85$, for various t' and $\delta t/t$.

system is monotonic with respect to strain. For $t' \geq 0$ the response function is non-linear for across the temperature range and for $t' = 0.2$, is increasingly non-linear with warming.

3. Strain-Kinetic-Energy Susceptibility versus strain

In Fig. 11, we present the strain-kinetic-energy susceptibilities versus strain at optimal density ($n = 0.85$) and $t' = 0.2t$ for A_{1g} , B_{1g} , XX and YY where we define the longitudinal and transverse response functions as

$$M_{XX} \equiv -\left(\frac{K'_{xx} - K_{xx}}{K_{xx}}\right) / \left(\frac{\delta t}{t}\right), \quad (52)$$

$$M_{YY} \equiv -\left(\frac{K'_{yy} - K_{yy}}{K_{xx}}\right) / \left(\frac{\delta t}{t}\right). \quad (53)$$

respectively. Here, we can examine the linearity of the response function at a fixed T . We note that a horizontal

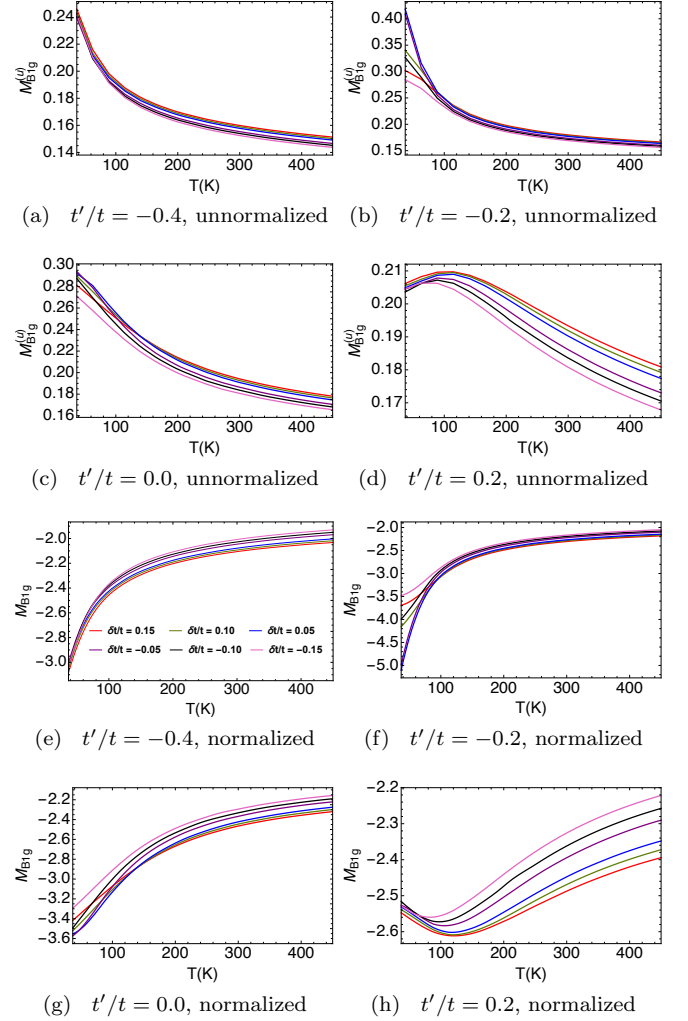


FIG. 10: The strain-kinetic-energy susceptibilities for the B_{1g} irrep at filling $n = 0.85$ for various t' and $\delta t/t$. (a)-(d) unnormalized susceptibilities, Eq. (51). (e)-(h) the normalized susceptibilities, Eq. (50). All figures share a legend.

line shape is characteristic of a linear function, a sloped line is indicative of a second order term and a non-zero curvature signals higher order terms. For A_{1g} , we observe that the irrep is weakly non-linear up to room temperature, it grows increasingly non-linear as the system is cooled and the curve is anti-symmetric with respect to hopping strain. For the B_{1g} irrep, we note that the response function is linear at room temperature; however, it becomes non-linear at the temperature is dropped, but in this case the response function is symmetric with respect to strain. The A_{1g} irrep corresponds to the scale of the total optical conductivity, $\sigma_{xx} + \sigma_{yy}$, and it indicates that the total optical conductivity increases as we go from a tensile strain to a compressive strain. The B_{1g} irrep signals whether the kinetic energy anisotropic, i.e., a non-zero response indicates that the kinetic energy is more sensitive either in the longitudinal or transverse direction. The anti-symmetry of A_{1g} together with the

symmetry of B_{1g} tell us that the sensitivity is symmetric for compressive and tensile strains. In comparing panels (b), (c), and (d) we see strong similarity between their respective responses. This is expected since strain merely shifts kinetic energy versus temperatures curves up and down.

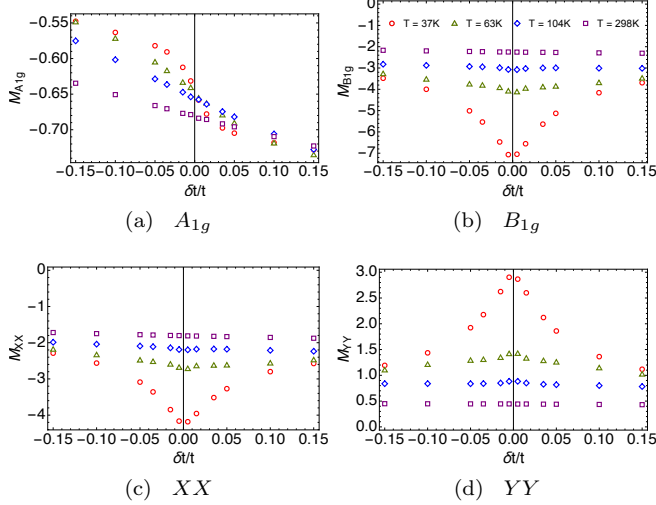


FIG. 11: The strain-kinetic-energy susceptibilities versus strain at filling $n = 0.85$ and $t'/t = -0.2$ at four representative temperatures. All figures share a legend. (a) A_{1g} irrep, Eq. (48). (b) B_{1g} irrep, Eq. (50). (c) XX , longitudinal, Eq. (52). (d) YY , transverse, Eq. (53).

C. The local density of states for an x-axis strain

The local density of states (LDOS) is potentially interesting since it can be measured using STM probes. We present results on how the LDOS changes with strain, and the related susceptibilities. We argue that if experiments are done on resistivity variation as well as LDOS variation with strain, we can bypass the need for measuring strain accurately and of estimating the parameter α in Eq. (14). The LDOS is calculated as $\rho_{G_{\text{loc}}}(\omega) = \langle \rho_G(\mathbf{k}, \omega) \rangle_{\mathbf{k}}$ where averaging over the Brillouin zone is implied, and $G \rightarrow g$ is the free Greens function for the bare LDOS and the ECFL Greens function $G \rightarrow \mathcal{G}$ for the LDOS in the non-trivial case.

In this section we calculate the normalized change in the local density of states and quote the following:

- $\rho'_{g_{\text{loc}}}(k)$, this is the strained version of the bare LDOS.
- $\rho'_{G_{\text{loc}}}(k)$, this is the strained version of the interacting LDOS.
- We call $\rho_{g_{\text{loc}}}$ without a prime as the tetragonal result and similarly for $\rho_{G_{\text{loc}}}$.
- We present $(\rho'_{g_{\text{loc}}} - \rho_{g_{\text{loc}}})/(\rho_{g_{\text{loc}}}\delta t/t)$ vs ω

- We present $(\rho'_{G_{\text{loc}}} - \rho_{G_{\text{loc}}})/(\rho_{G_{\text{loc}}}\delta t/t)$ vs ω

1. T variation

In Fig. 12, we display the LDOS at optimal density ($n = 0.85$) and $t' = -0.2$ for various temperatures at three characteristic strains: a compressive strain (thick dashed), unstrained (solid) and tensile strain (thin dashed). We compare the LDOS for non-interacting system, panel (a), to a system with electron-electron interaction, panel (b)-(d). We find that curve for the bare LDOS shifts to left along the ω -spectrum upon warming, leaving the line shape intact. In contrast with the bare LDOS, we see that warming the LDOS for the interacting system completely smooths and broadens the LDOS peaks for all strains rather than shifting them left. We note that strain inverts the LDOS peak, leaving behind a pair of cusps at a reduced height. This is a product of the anisotropy of hopping parameters. This is consistent with previous findings that interaction significantly lower the Fermi liquid temperature T_{FL} ³².

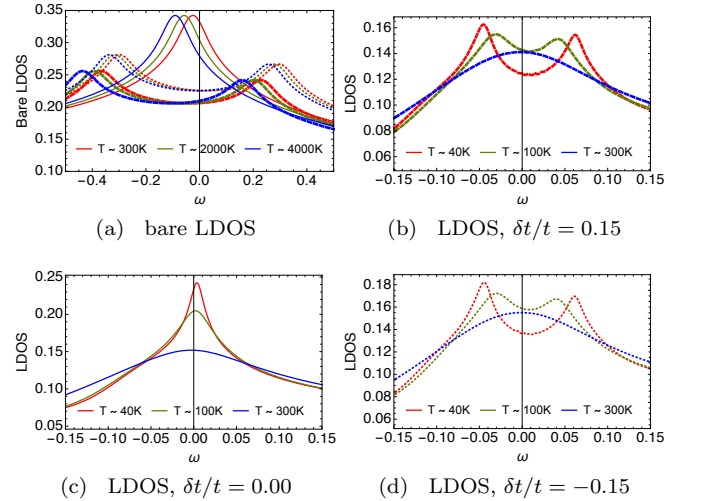


FIG. 12: The local density of states for (a) the non-interacting and (b)-(d) interacting system at optimal filling ($n = 0.85$), $t' = -0.2$, for various temperatures and at three characteristic strains: $\delta t/t = 0.15, 0.00, -0.15$ (thick dashed, solid, thin dashed).

2. t' variation

In Fig. 13, we examine the LDOS from a different vantage point by looking at the t' dependence for a system at optimal density ($n = 0.85$), for a compressive strain of $\delta t/t = 0.15$, and at various $t'/t = -0.4, -0.2, 0.0, 0.2$. In panel (c), we show the bare LDOS under at room temperature as a reference for the interacting system. In panels (a) and (b), we display interacting system at $T = 37\text{K}$ and $T = 298\text{K}$, respectively. Upon inspection it appears

the primary role that t' plays is to shift energy band along the spectrum. As previously noted, warming the interacting system to room temperature smooths and broadens the characteristic LDOS peaks for all strain types and at all t' while leaving their position the spectrum fixed. Even though the relative position of different t' curves remain unchanged as the interactions are turned on, we note that strong correlations renormalizes the bare band into a smaller energy region. Comparing panels (a) and (b) fixed at $t' = -0.4, 0.2$, we observe that LDOS peak height is more strongly suppressed at a lower t' . This is consistent with previous studies on the unstrained interacting system, and it indicates that a smaller t' has a lower Fermi-liquid temperature scale and hence it is less robust to heating.

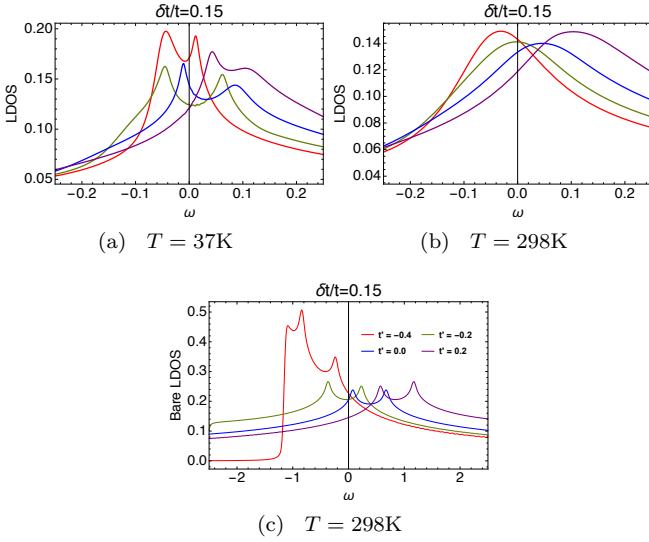


FIG. 13: The local density of states versus frequency at optimal filling ($n = 0.85$), for a compressive strain ($\delta t/t = 0.15$) at various t' . (a)-(b) The interacting system at $T = 37\text{K}$ and $T = 298\text{K}$, respectively. (c) The non-interacting system at $T = 298\text{K}$. All figures share the same legend.

3. Susceptibilities

In this section, we examine the normalized response function of LDOS of the non-interacting and interacting system, respectively, defined as

$$N_g \equiv \left(\frac{\rho'_{g\text{loc}} - \rho_{g\text{loc}}}{\rho_{g\text{loc}}} \right) / \left(\frac{\delta t}{t} \right), \quad (54)$$

$$N_G \equiv \left(\frac{\rho'_{G\text{loc}} - \rho_{G\text{loc}}}{\rho_{G\text{loc}}} \right) / \left(\frac{\delta t}{t} \right). \quad (55)$$

In Fig. 14, we plot the LDOS susceptibility for a non-interacting and interacting system at room temperature at optimal density for various t' . We observe that the response function is linear at all frequencies except at the

LDOS peak and, although not shown in the figure, at the band edges. Regardless of the presence of interaction, we note that the susceptibility is enhanced by tensile strain near the LDOS peak and reduced by a compressive strain.

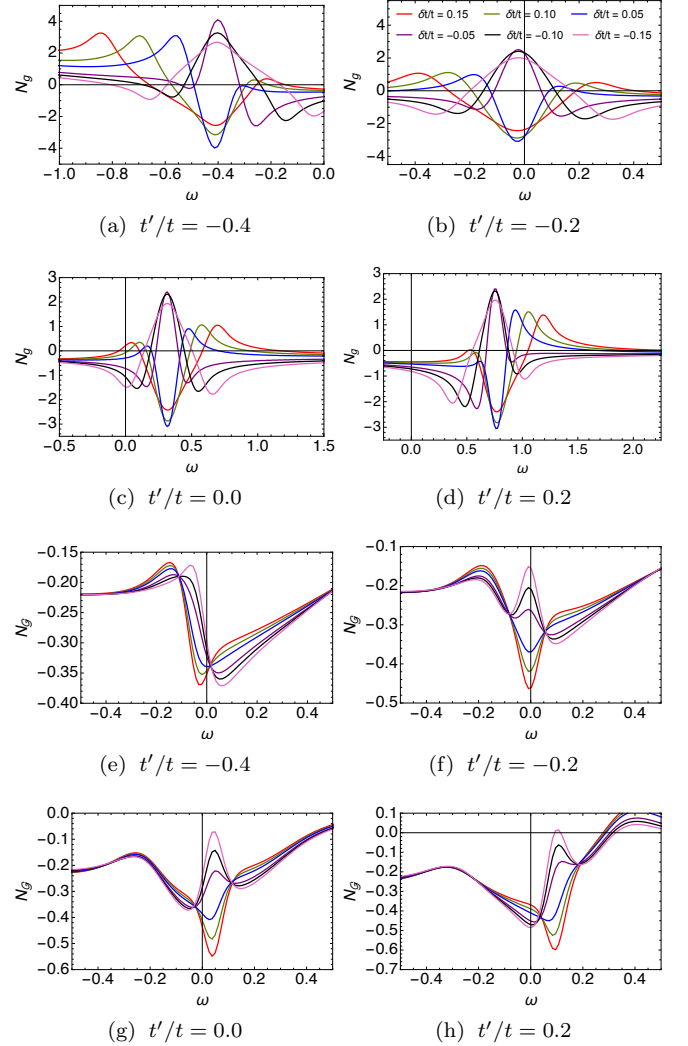


FIG. 14: The LDOS susceptibility versus frequency at optimal filling $n = 0.85$, at room temperature ($T = 297\text{K}$), for various t' and $\delta t/t$. (a)-(d) The non-interacting system, Eq. (54). (e)-(h) The interacting system, Eq. (55). All the figures share a legend.

4. Susceptibility versus strain

In Fig. 15, we display the LDOS susceptibility as function of strain, at four representative frequencies. A curve that is constant is characteristic of a linear response function. We see that at $\omega = 0$ the response function is non-linear to second order.

We can approximate the response function in Eqs. (54)

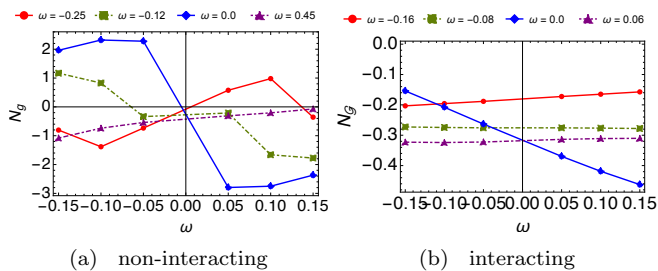


FIG. 15: The LDOS susceptibility versus strain at optimal filling $n = 0.85$, at room temperature ($T = 298K$), for $t' = -0.2t$, at a few representative frequencies ω in units of t . (a) The non-interacting system, Eq. (54). (b) The interacting system, Eq. (55).

and (55) as

$$N(n, T) = c_0 + c_1 \delta t/t + c_3 (\delta t/t)^2 + \dots \quad (56)$$

where c_0 is the linear response term, c_1 is the quadratic response term and c_2 is the third order term. We see that for the bare LDOS, Fig. 15(a), at $\omega = 0.45$ the system is nearly linear with $c_0 \approx -0.5$ and $c_1 \approx 3$. The other presented frequencies appear to be non-linear with significant second and third order terms. The LDOS susceptibility for interacting system, panel (b), appears to be nearly linear everywhere except at the location of LDOS peak ($\omega = 0$) which has weak second order term. Note that the second order scheme used here is good for low energies but somewhat less reliable at high energies, $|\omega| \gtrsim t$.

IV. CONCLUSION & DISCUSSION

In this work, we have applied the recently developed second-order ECFL theory to study the effect of small strain on the resistivity, kinetic energy, LDOS and their associated susceptibilities in the t - t' - J model with various t' at $n = 0.85$ and 0.80 .

The second order scheme of ECFL used here seems to be quite accurate for electron density $.82 \leq n \leq .87$, as shown in our earlier studies by comparison with other schemes. It must be kept in mind that the presented results are not exact within ECFL. As explained in Ref. [11,28,31], higher order terms in the λ expansion and alternate treatment of the two number sum-rules, are ex-

pected to change the high energy (i.e. $|\omega| \gg k_B T_{FL}$) response functions substantially. The low energy response (i.e. $|\omega| \lesssim k_B T_{FL}$) involved in the resistivity calculations is not expected to change too much. We are currently also pursuing directions for such improvement of the calculational scheme. While resistivities themselves might not change too much, the related susceptibilities are more sensitive, and hence we might see greater changes. However comparison of the present scheme with experiments seems warranted already, at least to provide some guidance to experiments for the signs and scales of variations.

Our results exhibit in considerable detail the variation of the strain dependence, and the sign and magnitude t' on resistivities and other variables. This implies that electron doped and hole doped cases behave very differently. Further the magnitude of t' distinguishes between different members of the hole doped materials. In comparing with the strain variation data, when it becomes available, one would need to estimate the magnitude of t' from the T dependence of the unstrained resistivity, before embarking on an exploration of the strain dependence.

Our results can be converted to actual strains by replacing $\delta t/t$ with $-\alpha \delta R/R$ using Eq. (17), or better still, by measuring the strain dependence of the LDOS or the optical conductivity sum-rule, and thereby eliminating α . In practice one might also choose typical values of $\alpha \sim 5 \pm 2$ to get useful estimates.

It should be noted that while typical experimental conditions (e.g. from applying in-plane uni-axial stress) will typically result in normal strains in x, y and z directions, with ratios given by Poisson ratios etc, nevertheless, the symmetry-decomposed response (at least for small strains) can still be extracted from the calculations and compared with symmetry-decomposed responses in real materials. Of course the c-axis strain (an A_{1g} quantity for a tetragonal material) can affect the in-plane isotropic (A_{1g}) elasto-resistivity as well as the in-plane A_{1g} strain. Our model is strictly 2d, so it won't capture this.

§Acknowledgement: We thank Ian Fisher and Steve Kivelson for stimulating our interest in this problem, and for helpful discussions. The work at UCSC was supported by the US Department of Energy (DOE), Office of Science, Basic Energy Sciences (BES), under Award No. DE-FG02-06ER46319. The computation was done on the comet in XSEDE⁴² (TG-DMR170044) supported by National Science Foundation grant number ACI-1053575.

¹ Y. Onose, Y. Taguchi, K. Ishizaka, and Y. Tokura, Phys. Rev. B **69**, 024504 (2004).

² R. L. Greene, P. R. Mandal, N. R. Poniatowski and T. Sarkar, [arXiv:1905.04998](https://arxiv.org/abs/1905.04998) (2019).

³ Y. Ando, S. Komiyama, K. Segawa, S. Ono, and Y. Kurita, Phys. Rev. Lett. **93**, 267001 (2004).

⁴ G. Kotliar, S. Y. Savrasov, K. Haule, V. S. Oudovenko, O.

Parcollet and C. A. Marianetti, Rev. Mod. Phys. **78** 865 (2006).

⁵ W. Xu, K. Haule, and G. Kotliar, Phys. Rev. Lett. **111**, 036401 (2013).

⁶ X.Y. Deng, J. Mravlje, R. Žitko, M. Ferrero, G. Kotliar and A. Georges, Phys. Rev. Lett. **110**, 086401 (2013).

⁷ K. Bouadim, N. Paris, F. Hebert, G. G. Batrouni, and R.

- T. Scalettar, Phys. Rev. B **76**, 085112 (2007).
- ⁸ E. W. Huang, R. Sheppard, B. Moritz and T. P. Devereaux, [arXiv:1806.08346v2](https://arxiv.org/abs/1806.08346v2) (2019).
- ⁹ T. A. Maier, M. Jarrell, T. Prushke, and M. H. Hettler, Rev. Mod. Phys. **77**, 1027 (2005).
- ¹⁰ Y. Zhang, Y. F. Zhang, S. X. Yang, K.-M. Tam, N. S. Vidhyadhiraja and M. Jarrell Phys. Rev. B **95** 144208 (2017).
- ¹¹ B. S. Shastry and E. Perepelitsky, [arXiv:1605.08213](https://arxiv.org/abs/1605.08213). Phys. Rev. B **94**, 045138 (2016); R. Žitko, D. Hansen, E. Perepelitsky, J. Mravlje, A. Georges and B. S. Shastry, [arXiv:1309.5284](https://arxiv.org/abs/1309.5284) (2013), Phys. Rev. B **88**, 235132 (2013); B. S. Shastry, E. Perepelitsky and A. C. Hewson, [arXiv:1307.3492](https://arxiv.org/abs/1307.3492), Phys. Rev. B **88**, 205108 (2013).
- ¹² G. -H. Gweon, B. S. Shastry, and G. D. Gu, Phys. Rev. Lett. **107**, 056404 (2011).
- ¹³ A. Damascelli, Z. Hussain, and Z-X Shen, Rev. Mod. Phys. **75**, 473 (2003).
- ¹⁴ W. S. Lee, I. M. Vishik, D. H Lu and Z-X Shen, J. Phys.: Condens. Matter **21**, 164217 (2009).
- ¹⁵ J. D. Koralek, J. F. Douglas, N. C. Plumb, Z. Sun, A. V. Federov, M. M. Murnane, H. C. Kapteyn, S. T. Cundiff, Y. Aiura, K. Oka, H. Eisaki, and D. S. Dessau, Phys. Rev. Lett. **96**, 017005 (2006).
- ¹⁶ T. Yoshida, X. J. Zhou, D. H. Lu, S. Komiya, Y. Ando, H. Eisaki, T. Kakeshita, S. Uchida, Z. Hussain, Z-X Shen and A. Fujimori, J. Phys.: Condens. Matter **19** 125209 (2007).
- ¹⁷ N. P. Armitage, D. H. Lu, C. Kim, A. Damascelli, K. M. Shen, F. Ronning, D. L. Feng, P. Bogdanov, X. J. Zhou, W. L. Yang, Z. Hussain, P. K. Mang, N. Kaneko, M. Greven, Y. Onose, Y. Taguchi, Y. Tokura, and Z.-X. Shen, Phys. Rev. B **68** 064517 (2003).
- ¹⁸ P. Mai and B. S. Shastry, Phys. Rev. B **98**, 115101 (2018).
- ¹⁹ A. Koitzsch, G. Blumberg, A. Gozar, B. S. Dennis, P. Fournier, and R. L. Greene, Phys. Rev. B **67** 184522 (2003).
- ²⁰ W. Ding, R. Žitko, P. Mai, E. Perepelitsky and B. S. Shastry, [arXiv:1703.02206v2](https://arxiv.org/abs/1703.02206v2), Phys. Rev. B **96**, 054114 (2017); W. Ding, Rok Žitko, and B. S. Shastry, Phys. Rev. B **96**, 115153 (2017).
- ²¹ F. Ming, S. Johnston, D. Mulugeta, T. S. Smith, P. Vilmercati, G. Lee, T. A. Maier, P. C. Snijders, and H. H. Weiering, Phys. Rev. Lett. **119**, 266802 (2017).
- ²² Y. J. Yan, M. Q. Ren, H. C. Xu, B. P. Xie, R. Tao, H. Y. Choi, N. Lee, Y. J. Choi, T. Zhang, and D. L. Feng, Phys. Rev. X **5**, 041018 (2015).
- ²³ P. Choubey, A. Kreisel, T. Berlijn, B. M. Andersen, and P. J. Hirschfeld, Phys. Rev. B **96**, 174523 (2017).
- ²⁴ A. Kreisel, P. Choubey, T. Berlijn, W. Ku, B. M. Andersen, and P. J. Hirschfeld, Phys. Rev. Lett. **114**, 217002 (2015).
- ²⁵ K. Fujita, A. R. Schmidt, E. -A. Kim, M. J. Lawler, D. H. Lee, J. C. Davis, H. Eisaki, and S. -i. Uchida, J. Phys. Soc. Jpn. **81**, 011005 (2012).
- ²⁶ D. N. Basov and T. Timusk, Rev. Mod. Phys. **77**, 721 (2005).
- ²⁷ D. N. Basov, R. D. Averitt, D. van der Marel, M. Dressel, and K. Haule, Rev. Mod. Phys. **83**, 471 (2011).
- ²⁸ B.S. Shastry, Phys. Rev. Lett. **107**, 056403 (2011) <http://physics.ucsc.edu/~sriram/papers/ECFL-Reprint-Collection.pdf>
- ²⁹ B. S. Shastry, Phys. Rev. B **87**, 125124 (2013)
- ³⁰ B. S. Shastry, [arXiv:1312.1892](https://arxiv.org/abs/1312.1892) (2013), Ann. Phys. **343**, 164-199 (2014). (Erratum) Ann. Phys. Vol. 373, 717-718 (2016).
- ³¹ P. Mai and B. S. Shastry Phys. Rev. B **98**, 205106 (2018)
- ³² B. S. Shastry and P. Mai, New J. Phys. **20** 013027 (2018)
- ³³ V. Heine, Phys. Rev. **153**, p. 673 (1967).
- ³⁴ P. W. Anderson, Science **235**, 1196 (1987).
- ³⁵ M. Ogata and H. Fukuyama *Rep. Prog. Phys.* **71**, 036501 (2008).
- ³⁶ M. Tinkham, *Group Theory and Quantum Mechanics* (McGraw-Hill, 1964)
- ³⁷ M. Hamermesh, *Group Theory And Its Application To Physical Problems* (Addison-Wesley Pub. Co., 1962)
- ³⁸ L. D. Landau, & E. M. Lifshitz, Vol. 3. *Quantum Mechanics: Non-Relativistic Theory*, 3rd edition, (Elsevier, 1991), p. 366
- ³⁹ M. C. Shapiro, P. Hlobil, A. T. Hristov, A. V. Maharaj, and I. R. Fisher, Phys. Rev. B **92**, 235147 (2015)
- ⁴⁰ P. Mai, S. R. White and B. S. Shastry, Phys. Rev. B **98**, 035108 (2018).
- ⁴¹ The unstrained system assumes a body-centered orthorhombic unit cell (a, b, c) where a b are the lattice constants of the base and c is that of the height. In the expression for resistivity ρ_0 , c_0 corresponds to the interlayer separation $c_0 = c/2$ between copper-oxide planes.
- ⁴² J. Town et al., “XSEDE: Accelerating Scientific Discovery”, Computing in Science & Engineering, Vol.16, No. 5, pp. 62-74, Sept.-Oct. 2014, doi:10.1109/MCSE.2014.80

Supplementary Material: Theory of strain induced anisotropic resistivity of extremely strongly correlated metals in two dimensions

Michael Arciniaga¹, Peizhi Mai^{2,1}, B Sriram Shastry¹

¹*Physics Department, University of California, Santa Cruz, CA 95064, USA and*

²*Center for Nanophase Materials Sciences, Oak Ridge National Laboratory, Oak Ridge, TN, 37831-6494, USA*

(Dated: May 19, 2022)

I. OVERVIEW

The Supplementary Material (SM) section is organized as follows: In Sec. II A we expand upon the resistivity calculation by discussing the role of different terms on the resistivity calculation under an x-axis strain. In Sec. II B we examine the effects of strain on the total kinetic energy versus T , the longitudinal and transverse components versus T , and we display the effect of strain at the particle densities $n = 0.80, 0.85$. In Sec. II C we present supplemental figures showing the effects of strain on the local density of states (LDOS) and the LDOS susceptibilities for both non-interacting and interacting systems.

II. RESULTS

A. Resistivity for an x-axis strain : role of different factors

We further explore the effects of strain on electrical resistivity and their associated susceptibilities in response to an x-axis strain for an extremely correlated Fermi liquid^{SM-1,SM-2} (ECFL). In order to gauge the relative importance of strain in the resistivity calculation^{SM-3}, it is useful to study the effect of strain on each term in conductivity calculation:

$$\sigma_{xx} = \left\langle \Upsilon_{\mathbf{k}} \left(\frac{\partial \epsilon_{\mathbf{k}}}{\partial k_1} \right)^2 (a/b) \right\rangle_{\mathbf{k}}, \quad (\text{SM-1})$$

$$\sigma_{yy} = \left\langle \Upsilon_{\mathbf{k}} \left(\frac{\partial \epsilon_{\mathbf{k}}}{\partial k_2} \right)^2 (b/a) \right\rangle_{\mathbf{k}}. \quad (\text{SM-2})$$

Here, we note that strain affects conductivity in two fashions: it produces a change (1) in the lattice constant:

$$a \rightarrow a_0 + \delta a; \quad b \rightarrow a_0; \quad \rho \rightarrow \sqrt{2}a_0 + \frac{\delta a}{\sqrt{2}}, \quad (\text{SM-3})$$

and (2) in the hopping parameters:

$$t_x = (1 - \alpha \epsilon) t; \quad t_y = t; \quad t_d = (1 - \alpha \frac{\epsilon}{2}) t'. \quad (\text{SM-4})$$

The distorted lattice constants play the role of a dimensionless coefficient in Eqs. (SM-1) and (SM-2). The modified hopping parameters comes into play through the

vertices and the spectral function in $\Upsilon_{\mathbf{k}}$. Specifically, we compute the resistivity while isolating the effects of strain on the following terms: (1) the spectral functions in $\Upsilon_{\mathbf{k}}$, (2) the ‘‘vertex’’ $\partial \epsilon_{\mathbf{k}} / \partial k_i$ for $i = 1, 2$, and (3) the distorted lattice constants a, b , denoted ‘‘Geometric’’ in Fig. 1, and we record the sensitivity of conductivity to each term.

In SM-Fig. 1(a)-(b), we present the change in the longitudinal and transverse resistivity versus T , respectively, at filling $n = 0.85$, second neighbor hopping $t' = -0.2t$ and hopping strain $\delta t/t = 0.15$ for all three terms and we compare them to a resistivity calculation on the unstrained tetragonal lattice denoted ‘‘Tetra’’ and a calculation that combines the effects of strain on every term which we call ‘‘Ortho’’. We observe that the longitudinal resistivity is primarily sensitive to the effects of strain on the vertex. Panel (b) shows that the transverse resistivity is sensitive to the effect of strain on the spectral functions, i.e., $\Upsilon_{\mathbf{k}}$. In panels (c) and (d) we have the response function for the irrep A_{1g} and B_{1g} , respectively^{SM-4}. As we might expect, these curves are sensitive to both the vertex part and the spectral function. We also note that the source of the T -dependence is the spectral function and that the dominate source of asymmetry between compressive and tensile strain for the A_{1g} and B_{1g} irreps is the vertex and Υ_k terms.

B. The kinetic energy under a x-axis strain

Now we look at the anisotropy of the kinetic energy for an ECFL under a strain along the x-axis. Recall that the anisotropic kinetic energy can be related to a measurement of the optical weight through the f-sum rule^{SM-6,SM-7} on the t - t' - J model, and it is an experimentally accessible observable.

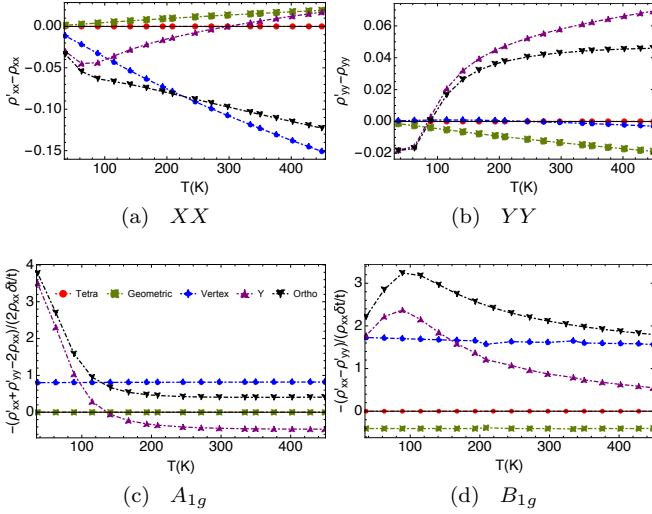
The total kinetic energy for a system under strain is computed as

$$K_{\text{tot}} = \left\langle \int_{-\infty}^{\infty} \rho_{\mathcal{G}}(k) \epsilon_{\mathbf{k}} d\omega \right\rangle_{\mathbf{k}}, \quad (\text{SM-5})$$

which may be decomposed as follows:

$$K_{\text{tot}} = K_{xx} + K_{yy} + K_{xy}, \quad (\text{SM-6})$$

where K_{xy} is the kinetic energy along the diagonal of orthorhombic lattice and is isotropic for each diagonal. Here we present the following susceptibilities:



SM-Fig 1: We gauge the sensitivity of different terms in Eqs. (SM-1) and (SM-2) to the effects of strain for various representations of the resistivity: (a) The change in longitudinal resistivity. (b) The change in transverse resistivity. (c) The resistivity for the A_{1g} irrep. (d) The resistivity for the B_{1g} irrep. The line The curve labeled “Geometric” gauges the sensitivity of resistivity to a direct change in lattice parameters a and b . The curve we call “Vertex” examines the effects of strain on $\partial\epsilon_{\mathbf{k}}/\partial k$ which is modified to be only a function of t, t' . The curve labeled “ Υ ” isolates the effects of strain on ρ_G . The curve labeled “Ortho” includes the effect of strain on every term. All figures share a legend. The parameters are set to filling $n = 0.85$, $t' = -0.2t$ and compressive strain of $\delta t/t = 0.15$.

- We present A_{1g} :

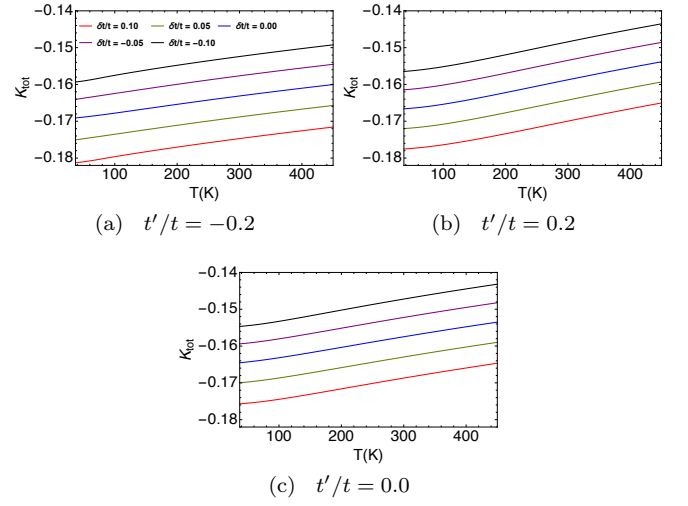
$$\frac{K'_{xx} + K'_{yy} - 2K_{xx}}{2K_{xx}\delta t/t} \text{ vs } T$$

- We present B_{1g} : $(K'_{xx} - K'_{yy})/(K_{xx}\delta t/t)$ vs T
- We present XX : $(K'_{xx} - K_{xx})/(K_{xx}\delta t/t)$ vs T
- We present YY : $(K'_{yy} - K_{yy})/(K_{xx}\delta t/t)$ vs T

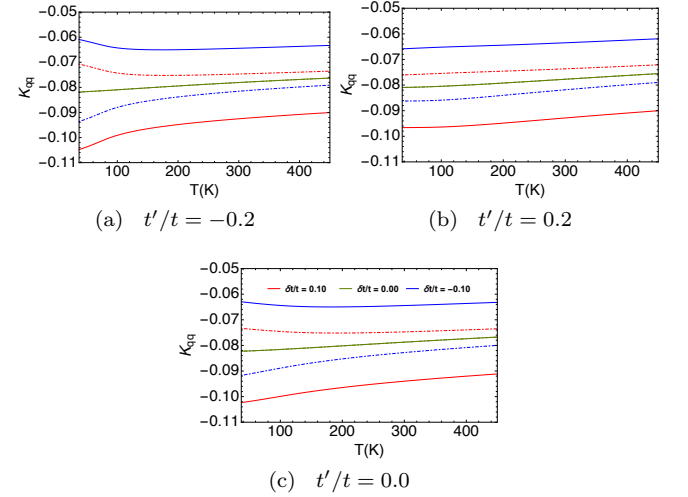
1. The raw kinetic energies

SM-Fig. 2 shows the total kinetic energy, K_{tot} , versus T at various t' and $\delta t/t$. We observe that decreasing the strain at a fixed T increases the total kinetic energy for all t' which indicates the scale of the optical conductivity increases as we decrease the strain is decreased. We also note that, similar to resistivity, the curvature of the line shape changes from negative to positive as t' increases for from negative (hole-like) to positive (electron-like).

In SM-Fig. 3, we display the longitudinal (solid) and the transverse (dashed) kinetic energy versus T at optimal density ($n = 0.85$) at various t' and for three representative strains: $\delta t/t = 0.10, 0.00, -0.10$. We observe

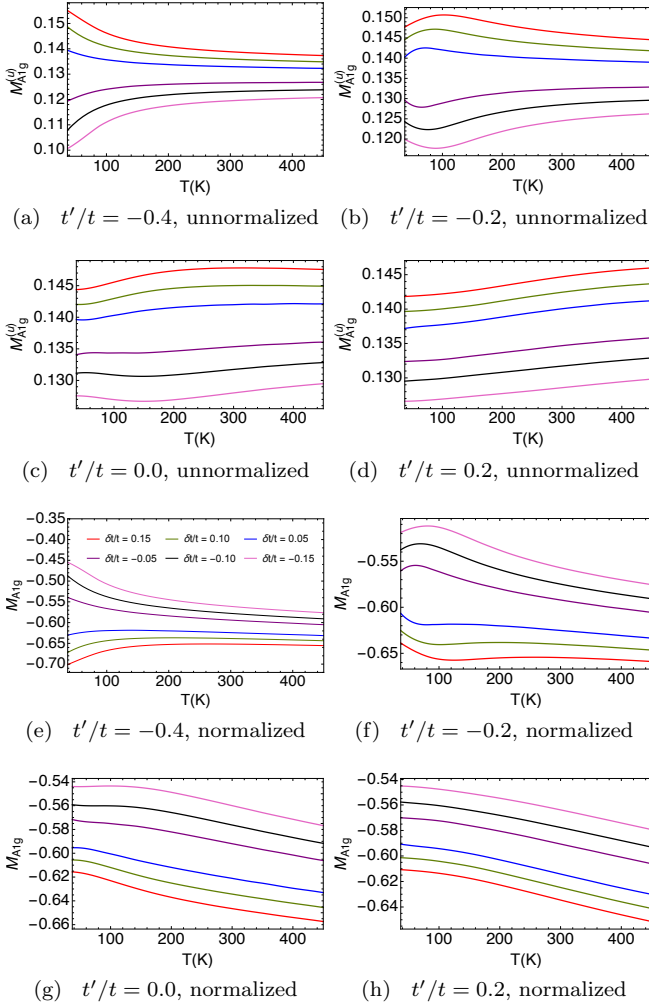


SM-Fig 2: The total kinetic energy at optimal filling $n = 0.85$, at various t' , for several $\delta t/t$. All figures shared a legend.



SM-Fig 3: The kinetic energy versus T where K_{xx} (solid) and K_{yy} (dashed) at optimal filling ($n = 0.85$), for various t' , and at three representative strains: compressive strain, no strain, tensile strain. Note that $K_{xx} = K_{yy}$ in the absence of strain. All figures share a legend.

that in the longitudinal direction the response to a compressive strain reduces the kinetic energy while a tensile strain enhances it, and we note that the response with respect to strain is less sensitive in the transverse direction and has the opposite sign. As the system is cooled, we find a slight increase in the sensitivity to strain at low temperatures. At low temperature, the kinetic energy slightly depends on t' , namely, it decreases as t' goes from positive (electron-like) to negative (hole-like), but as the system is warmed to room temperature, it becomes nearly independent of t' .



SM-Fig 4: The unnormalized (Eq. (SM-7)) and normalized (Eq. (SM-8)) strain-kinetic-energy susceptibilities for the A_{1g} irreducible representations at optimal filling $n = 0.80$ for various t' and $\delta t/t$. All figures share a legend.

2. Strain-kinetic-energy susceptibilities for the A_{1g} irrep

In SM-Fig. 4, we examine the unnormalized and normalized strain-kinetic-energy susceptibilities versus temperature in the A_{1g} irrep at over-doped density ($n = 0.80$) for various t' and $\delta t/t$. We define the unnormalized and normalized response function for the strain-kinetic-energy, respectively, as

$$M_{A_{1g}}^{(u)} \equiv -\left(K'_{xx} + K'_{yy} - 2K_{xx}\right) / \left(\frac{\delta t}{t}\right), \quad (\text{SM-7})$$

$$M_{A_{1g}} \equiv -\left(\frac{K'_{xx} + K'_{yy} - 2K_{xx}}{2K_{xx}}\right) / \left(\frac{\delta t}{t}\right). \quad (\text{SM-8})$$

In the normalized cases in SM-Fig. 4(e)-(h), we observe that the response functions is non-linear throughout the displayed temperature range for all t' . The even spacing between curves at different hopping strains indicates that these are second-order response functions. We also

notice that the response function monotonically increases in absolute intensity as the system warms or as the strain increases from negative to positive.

3. Strain-Kinetic-Energy susceptibilities with B_{1g} symmetry

In SM-Fig. 5 we display the unnormalized and normalized strain-kinetic-energy susceptibility versus T at over-doped density ($n = 0.80$) at various t' for the B_{1g} irrep of the D_{h4} point group, which is characterized as the difference in the kinetic energies $K_{xx} - K_{yy}$ along the different directions of the distorted square lattice. We define the response function of the kinetic energy for the B_{1g} irrep for the unnormalized and normalized, respectively, as

$$M_{B_{1g}}^{(u)} \equiv -\left(K'_{xx} - K'_{yy}\right) / \left(\frac{\delta t}{t}\right), \quad (\text{SM-9})$$

$$M_{B_{1g}} \equiv -\left(\frac{K'_{xx} - K'_{yy}}{K_{xx}}\right) / \left(\frac{\delta t}{t}\right). \quad (\text{SM-10})$$

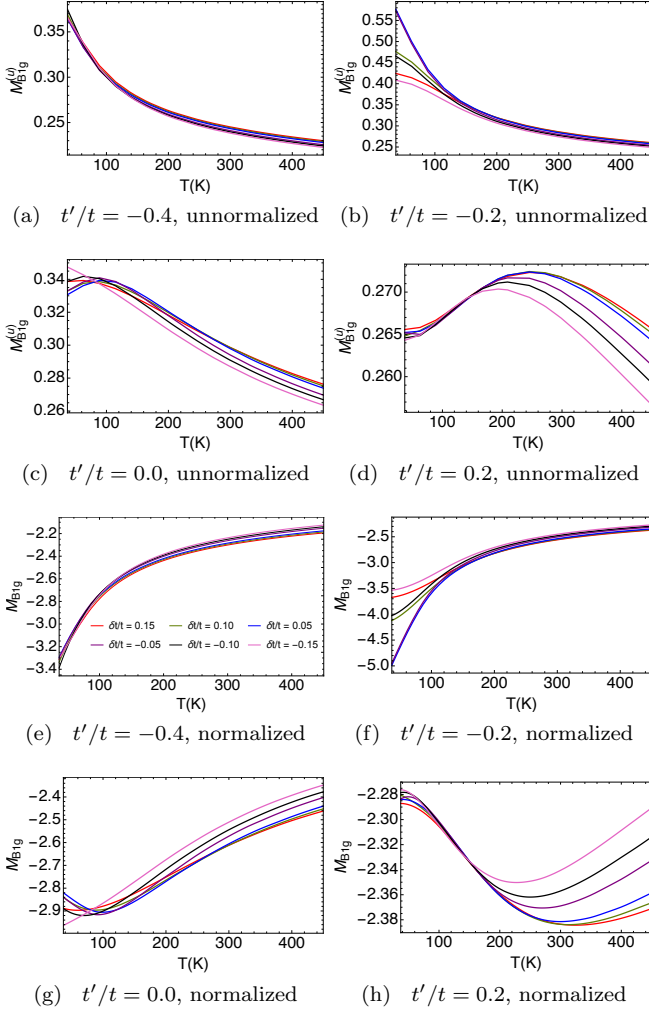
4. The longitudinal and transverse strain-kinetic-energy susceptibilities

In this section, we denote the strain-kinetic-energy susceptibility for the longitudinal and transverse directions, respectively, as

$$M_{XX} \equiv -\left(\frac{K'_{xx} - K_{xx}}{K_{xx}}\right) / \left(\frac{\delta t}{t}\right), \quad (\text{SM-11})$$

$$M_{YY} \equiv -\left(\frac{K'_{yy} - K_{yy}}{K_{xx}}\right) / \left(\frac{\delta t}{t}\right). \quad (\text{SM-12})$$

In SM-Figs 6 and 7, we display the longitudinal [(a)-(d)] and transverse [(e)-(h)] strain-kinetic-energy susceptibilities versus temperature at two representative densities ($n = 0.80$ and $n = 0.85$, respectively) at various t' and $\delta t/t$. First, we note that as we increase the density towards the optimal limit the line shape of the response functions remains approximately unchanged; However, the strength of the transverse response increases, and at high temperatures it becomes increasingly linear. We also note that there is an approximate mirror symmetry between the longitudinal response and the transverse response. Although, the intensity of the transverse response is weaker which is consistent with the raw data. Now, let us focus on the longitudinal response at optimal density. We see that for all t' the longitudinal response is non-linear at all displayed temperatures. Next, we examine the transverse response function which is linear at room temperature and becomes increasingly non-linear as the system is cooled. For $t' = -0.2t$ the response function at low temperatures is weakly asymmetric with respect to a compressive and tensile strain for both the longitudinal and transverse kinetic energies whereas for all other t' the response function increases monotonically



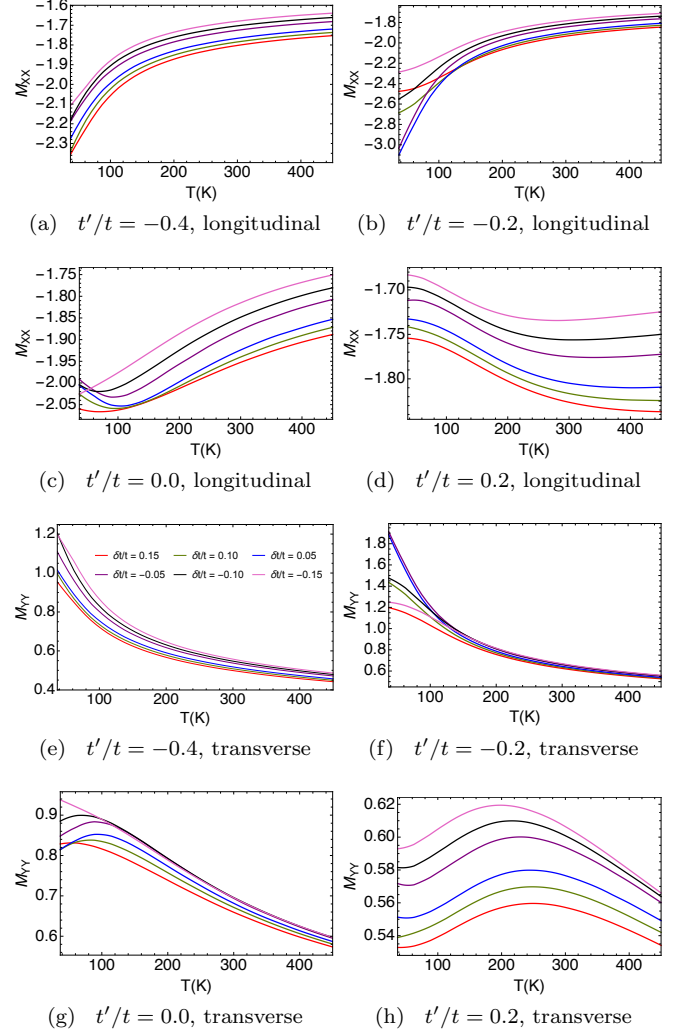
SM-Fig 5: The strain-kinetic-energy susceptibilities for the B_{1g} irreducible representation at over-doped filling $n = 0.80$, for various t' and $\delta t/t$. (a)-(d) The unnormalized susceptibilities, (Eq. (SM-9)). (e)-(h) The normalized susceptibilities, (Eq. (SM-10)). All figures share a legend.

with strain. And for $t' = 0.0, n = 0.80$ in SM-Fig. 6 (g), the transverse kinetic energy cannot resolve different tensile strains ($\delta t/t < 0.0$) until very low temperature while it is quite distinguishable in the compressive cases.

C. The Local Density of States

1. Strain variation

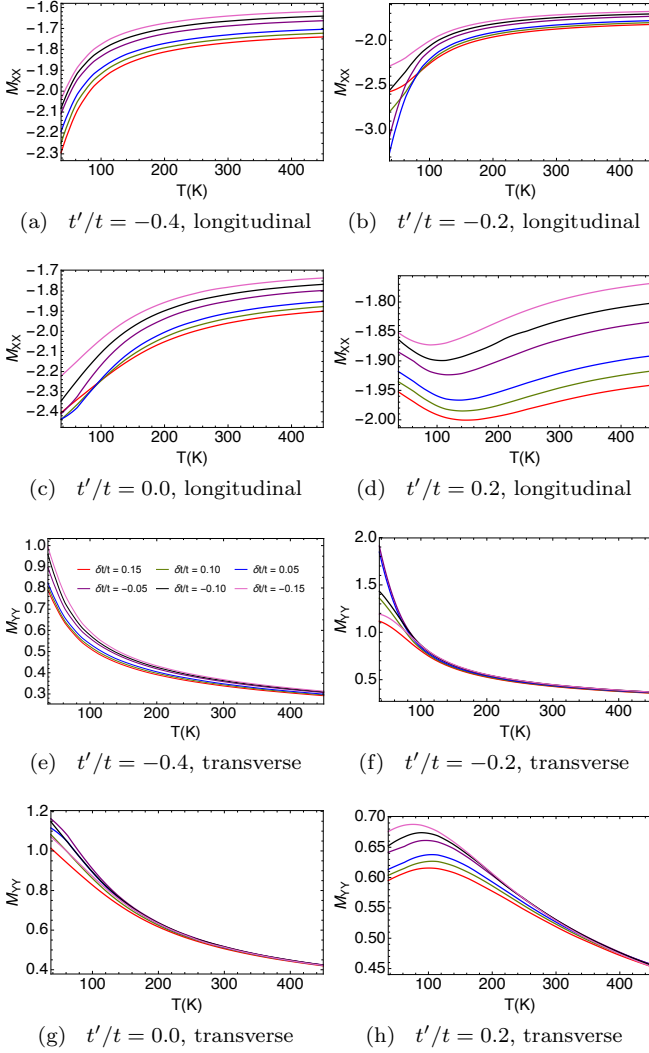
In SM-Figs. 8 and 9, we present the LDOS at over-doped density ($n = 0.80$) and optimal density ($n = 0.85$), respectively, at room temperature ($T = 298\text{K}$) for various t' and $\delta t/t$. Comparing these two figures, we note that the density has little effect beyond reducing the height of interacting system as it increases towards the Mott-insulating limit. Therefore, we will focus on analyzing



SM-Fig 6: The normalized strain-kinetic-energy susceptibilities for the longitudinal (Eq. (SM-11)) and transverse (Eq. (SM-12)) components at over-doped filling $n = 0.80$, for select t' , and $\delta t/t$. All figures share a legend.

SM-Fig. 8 since it applies to SM-Fig. 9 as well. In SM-Fig. 8 and 9 for the bare LDOS [(a)-(d)], we find that strain causes a highly localized inversion of the peak, resulting in a ‘well’ centered at same approximate position on the spectrum, surrounded by a pair of peaks at reduced height, where the lost weight is moved to the background.

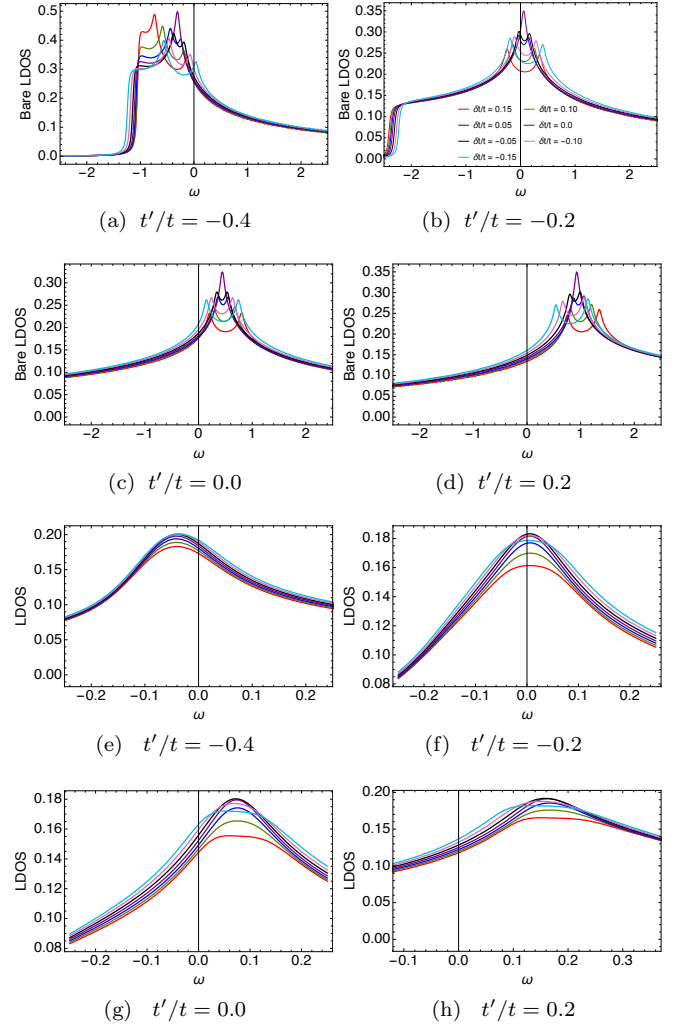
For $t'/t < 0$ ($t'/t > 0$) the bare LDOS peak heights are asymmetric, higher on the left (right), and shifted left (right) on the spectrum, and for $t'/t = 0$ the LDOS peaks are symmetric. We also notice an asymmetry between a compressive strain ($\delta t/t > 0$) and a tensile strain ($\delta t/t < 0$) where the bare LDOS peak height are more strongly inverted for the former except for $t'/t = -0.4$ since it is constrained by the band edge. In previous work^{SM-5}, it was shown that systems with high t' have higher Fermi liquid temperature scales, making them



SM-Fig 7: The normalized strain-kinetic-energy susceptibilities for longitudinal (Eq. (SM-11)) and transverse (Eq. (SM-12)) components optimal filling $n = 0.85$, for select t' , and $\delta t/t$. All figures share a legend.

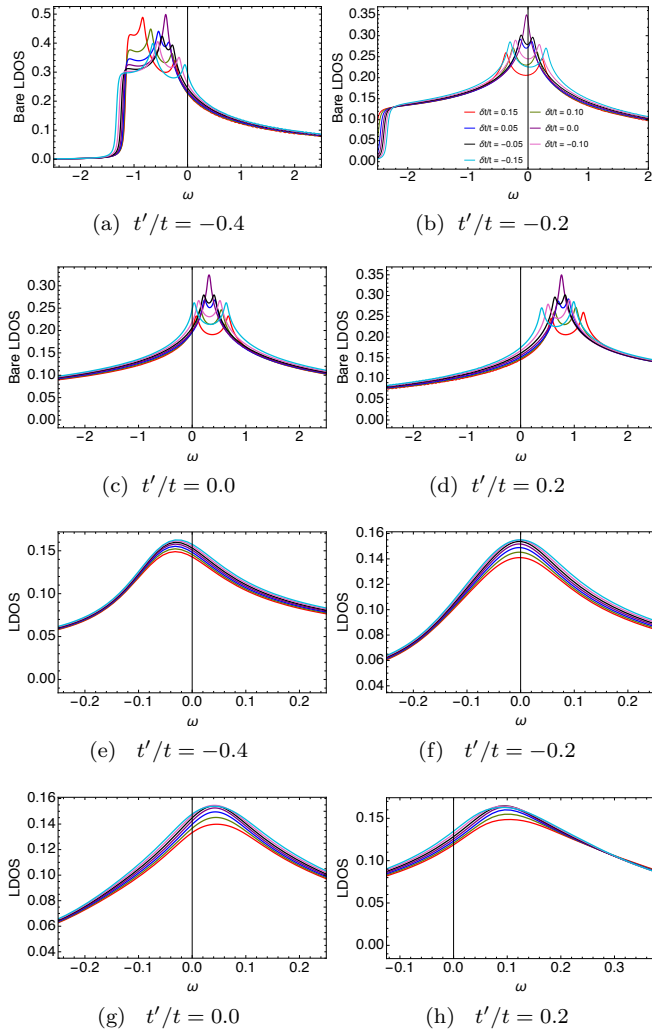
more robust to warming, that is, the LDOS peaks will have a slower rate of change (smoothing and broadening) in response to warming. Although we may expect the Fermi liquid temperature scale to warm as the hopping strain increases from negative (tensile) to positive (compressive), we find that the scale is similar for compressive and tensile strains of identical magnitude. This is a result of the anisotropy of the resistivity, producing two channels and hence two Fermi temperature scales. We propose the rate of change in LDOS peaks scales with the ratio $(t_d/t_x + t_d/t_y)/2$, where t_d/t_x and t_d/t_y determine the Fermi temperature scale for the longitudinal and transverse resistivity, respectively.

Now, in Fig. 8[(e)-(h)], we turn on the interaction and we observe that the LDOS peaks are smooth and broadened. In a previous study^{SM-5}, the authors showed that electron-electron interactions smooths and broadens the



SM-Fig 8: The local density of states versus frequency for at over-doped filling $n = 0.80$ at room temperature ($T = 298\text{K}$), for various $t' = -0.4, -0.2, 0.2, 0.0$ [clockwise], at select $\delta t/t$. (a)-(d) The non-interacting system. (e)-(h) The interacting system. All figures share a legend.

LDOS peak and that strong correlations packs the peaks for each t' into a smaller energy region while leaving the relative position ω spectrum unchanged. Here we find that strain inverts the line shape from a peak into a well while leaving the approximate position of different t' unchanged. Similar to the bare LDOS, we see that compressive strains tend to suppress the peak height and tensile strain tends to enhance it. This, again, is related to the T_{FL} scale as discussed above. If re-examining Fig. (12) in the main paper, we now note that at $T < T_{FL}$ the LDOS retains its characteristic double peak shape under strain. For $n = 0.85$ and $t' = -0.2t$, we find $T_{FL} < 150\text{K}$.



SM-Fig 9: The local density of states versus frequency at optimal filling $n = 0.85$, for room temperature ($T = 298\text{K}$), at various $t' = -0.4, -0.2, 0.2, 0.0$ at select $\delta t/t$. (a)-(d) The interacting system. (e)-(h) The non-interacting system. All figures share a legend.

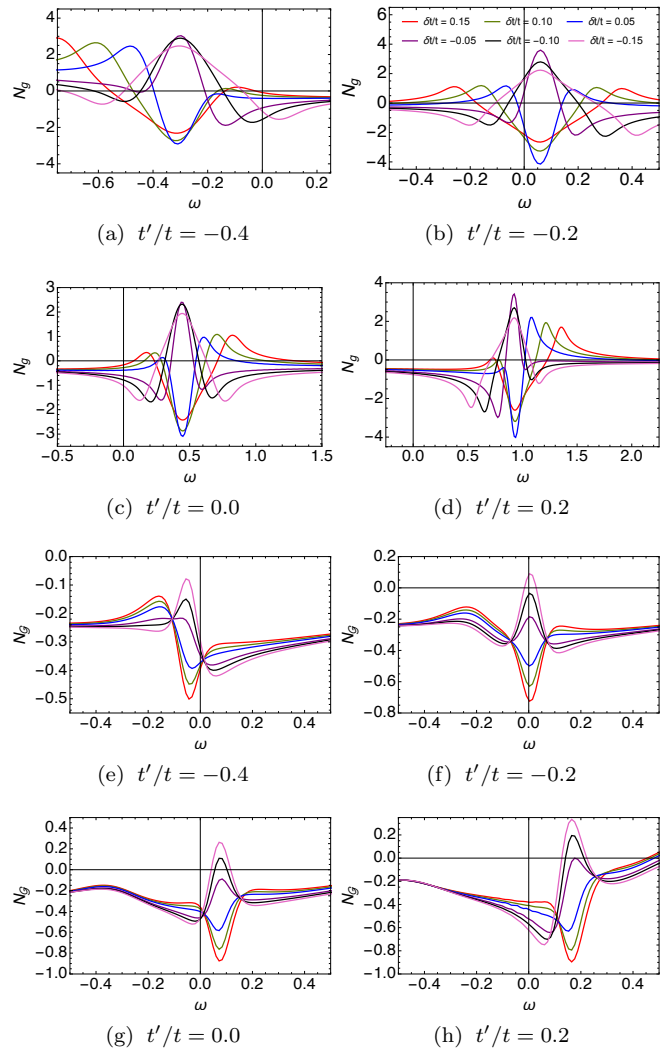
2. Susceptibilities

In SM-Fig. 10, we plot the LDOS susceptibility for an non-interacting and interacting system at room temperature at overdoped density, at various t' , for strains varying from $\delta t/t = -0.15$ – 0.15 . We define the non-interacting LDOS and the interacting LDOS response function, respectively, as

$$N_g \equiv \left(\frac{\rho'_{g\text{loc}} - \rho_{g\text{loc}}}{\rho_{g\text{loc}}} \right) / \left(\frac{\delta t}{t} \right), \quad (\text{SM-13})$$

$$N_G \equiv \left(\frac{\rho'_{G\text{loc}} - \rho_{G\text{loc}}}{\rho_{G\text{loc}}} \right) / \left(\frac{\delta t}{t} \right). \quad (\text{SM-14})$$

We observe that the location of the non-linear susceptibility coincides with the LDOS peak. Comparing the non-interacting LDOS [(a)-(d)] to the interacting LDOS [(e)-(h)] we find that the frequency region with non-linear behavior is more strongly localized for systems of the latter kind. A similar feature is observed for the location of LDOS peaks in unstrained systems after turning on interactions. We also find that, similar to the optimally doped system, in the over-doped system the susceptibility is enhanced by tensile strain and reduced by compressive strain regardless of the presence of interactions.



SM-Fig 10: The LDOS susceptibility versus frequency at overdoped filling $n = 0.80$, room temperature ($T = 298\text{K}$), for various t' and $\delta t/t$. (a)-(d) The non-interacting system, Eq. (SM-13). (e)-(g) The interacting system, Eq. (SM-14). All figures share a legend.

-
- [SM-1] B. S. Shastry, Phys. Rev. Lett. **107**, 056403 (2011). <http://physics.ucsc.edu/~sriram/papers/ECFL-Reprint-Collection.pdf>
- [SM-2] B. S. Shastry, Phys. Rev. B **87**, 125124 (2013).
- [SM-3] B. S. Shastry and P. Mai, New J. Phys. **20** 013027 (2018).
- [SM-4] M. C. Shapiro, P. Hlobil, A. T. Hristov, A. V. Maharaj, and I. R. Fisher, Phys. Rev. B **92**, 235147 (2015)
- [SM-5] P. Mai and B. S. Shastry, Phys. Rev. B **98**, 205106 (2018).
- [SM-6] D. N. Basov and T. Timusk, Rev. Mod. Phys. **77**, 721 (2005).
- [SM-7] D. N. Basov, R. D. Averitt, D. van der Marel, M. Dressel, and K. Haule, Rev. Mod. Phys. **83**, 471 (2011)